

# The effects of porosity in selective laser melted titanium inter-body cages and bone mineral density on subsidence.

A Biomechanical Study  
**Victoria Bruno**

Master of Science Thesis



**The effects of porosity in selective  
laser melted titanium interbody cages  
and bone mineral density on  
subsidence.  
A Biomechanical Study**

by

VICTORIA BRUNO

in partial fulfillment of the requirements for the degree of  
MASTER OF SCIENCE IN BIOMEDICAL ENGINEERING  
at Delft University of Technology to be defended publicly on  
August 23, 2019 at 14.00

Student number: 4628241

Thesis Committee: Dr. J. Zhou - Supervisor  
Ir. Pim Pellikaan - Supervisor (Amber Implants B.V.)  
Dr. Vera Popovich  
Dr. Mohammad Mirzaali

Faculty of Mechanical, Maritime and Materials Engineering (3mE) · Delft University  
of Technology

**amber** implants

The work in this thesis was supported by Amber Implants. Their cooperation is hereby gratefully acknowledged.



All rights reserved.

Copyright © BioMechanical Engineering

---

# Abstract

Degenerative disc disorders are among the most commonly diagnosed conditions and the leading cause for back and neck pain, affecting more than 266 million individuals annually. Interbody fusion is the proposed surgical treatment whenever lighter approaches such as physiotherapy and painkillers fail to improve the patient's condition. It consists of the total or partial removal of the damaged disc, followed by the insertion of a spinal implant, referred to as interbody fusion cage or spacer, to block the vertebral segment and restore disc height. Unfortunately, in some cases this treatment can fail due to a loss in disc height as a result of subsidence, that is the sinking of the cage in the adjacent vertebrae.

The investigation conducted in this thesis work focused on the effects of porosity of selective laser melted (SLM) implants and bone mineral density on subsidence, by means of a biomechanical study and a finite element model. In previous works, it was demonstrated that the most influential factor for the occurrence of subsidence is the condition of bone mineral density. Therefore, it was hypothesized that by using an implant with high porosity, the overall stiffness of the bone-implant system would decrease, as well as the stresses at the bone-implant interface, reducing the risk of subsidence and bone damage. At the same time, osseointegration would benefit due to the increased porosity, which is an important factor in the design of orthopedic implants. The biomechanical study consisted of compression tests according to the standard ASTM-F2267 for subsidence evaluation in interbody fusion implants, according to which polyurethane foams were used to simulate the mechanical behaviour of trabecular bone. Cages designated for the cervical and lumbar regions of the spine were tested in two different porosities, in terms of apparent density of the cage, in combination with three foam densities, low-medium- and high-density, corresponding respectively to low, average and above average quality of bone. The results confirmed the findings in the literature and revealed significantly different outcomes when the foam density was changed, while the change in porosity did not affect the stiffness of the foam-implant system. The finite element model of a simplified cervical cage was used to explore the influence of the thickness of the solid frame in porous implants, revealing changes in stiffness of the simulations with

the cages alone, while almost no stiffness variations were detected in the simulations for the implant-foam systems.

Although the reduction of the stiffness of the system could not be achieved by tuning porosity, it was demonstrated that the mechanical performance of the system was not affected by an implant with higher porosity. These findings opened new research opportunities in the study of osseointegration, since it could be concluded that the use of implants with higher porosity would not affect the overall stiffness, while allowing more bone ingrowth to avoid cage migration.

---

# Table of Contents

<b>Acknowledgements</b>	<b>xiii</b>
<b>1 Introduction</b>	<b>1</b>
1-1 Scope . . . . .	1
1-2 Structure of the report . . . . .	2
<b>2 The Spine</b>	<b>3</b>
2-1 The intervertebral disc . . . . .	3
2-1-1 Anatomy and physiology . . . . .	3
2-2 Pathophysiology and diseases . . . . .	5
2-3 Surgical treatments . . . . .	5
2-3-1 Static stabilization: Interbody fusion . . . . .	7
2-3-2 Dynamic stabilization . . . . .	10
<b>3 The Interbody Fusion Cage</b>	<b>11</b>
3-1 History . . . . .	11
3-2 Static and expandable cages . . . . .	13
3-3 Materials . . . . .	14
3-3-1 Titanium, PEEK and carbon fiber reinforced polymers . . . . .	14
3-3-2 Porous titanium and osseointegration . . . . .	15
3-4 Stand-alone cages and plating systems . . . . .	16
3-5 Device limitations . . . . .	17
<b>4 Thesis Rationale</b>	<b>21</b>
4-1 Overview . . . . .	21
4-2 Problem statement and research questions . . . . .	22

<b>5</b>	<b>Biomechanical Testing</b>	<b>23</b>
5-1	Standards for Interbody Fusion Devices . . . . .	23
5-1-1	ASTM-F2077 Test Methods for Intervertebral Body Devices . . . . .	23
5-1-2	ASTM-F2267 Standard Test Method for Measuring Load Induced Subsidence of an Intervertebral Body Fusion Device Under Static Axial Compression . . . . .	24
5-2	Test plan . . . . .	26
5-2-1	Sample preparation . . . . .	28
5-3	Test set-up . . . . .	29
5-3-1	Compression test for implant stiffness . . . . .	29
5-3-2	Compression test for subsidence . . . . .	31
5-3-3	Subsidence measurement . . . . .	31
5-4	Statistical Analysis . . . . .	31
5-5	Digital Image Correlation System . . . . .	33
<b>6</b>	<b>Computational Study</b>	<b>35</b>
6-1	Scope . . . . .	35
6-2	Geometries and material properties . . . . .	36
6-3	Interaction properties and boundary conditions . . . . .	38
6-3-1	Stiffness of the implant . . . . .	38
6-3-2	Stiffness of the implant-block system . . . . .	38
6-4	Mesh . . . . .	38
6-5	Limitations and assumptions . . . . .	39
<b>7</b>	<b>Results</b>	<b>41</b>
7-1	Biomechanical Study . . . . .	41
7-1-1	Stiffness of the implants . . . . .	41
7-1-2	Stiffness and yield load of the system . . . . .	42
7-1-3	Stiffness of the polyurethane foam blocks . . . . .	46
7-1-4	Subsidence . . . . .	47
7-1-5	Digital Image Correlation Data . . . . .	47
7-2	Computational Study . . . . .	50
7-2-1	Stiffness of the implants . . . . .	50
7-2-2	Stiffness of the implant-foam system . . . . .	51
7-2-3	Subsidence . . . . .	52

<b>8 Discussion</b>	<b>57</b>
8-1 Spinal cage porosity and bone density . . . . .	57
8-1-1 Mechanical properties of porous spinal cages . . . . .	57
8-1-2 Implications of the findings for the <i>in-vivo</i> performance . . . . .	58
8-1-3 Polyurethane foams for biomechanical tests of different bone densities . . . . .	59
8-2 Thickness of the cage frame in solid titanium . . . . .	62
8-3 Standalone cage and fixation systems . . . . .	63
8-4 ASTM-F2267: considerations and recommendations . . . . .	64
<b>9 Conclusion</b>	<b>67</b>
9-1 Biomechanical study . . . . .	67
9-2 Computational study . . . . .	68
9-3 Implications for the <i>in-vivo</i> performance of the implants . . . . .	68
<b>10 Recommendations</b>	<b>69</b>
10-1 Assessment of the implant location . . . . .	69
10-2 Assessment of bone mineral density . . . . .	69
10-3 Cell proliferation and growth . . . . .	70
10-4 Biomechanical study . . . . .	70
10-5 Computational study . . . . .	70
<b>Bibliography</b>	<b>71</b>
<b>Glossary</b>	<b>83</b>
List of Acronyms . . . . .	83
List of Symbols . . . . .	83



---

## List of Figures

2-1	Representation of a human spine. The curvature of the overall spine is called <i>lordosis</i> . At the cervical and lumbar regions the curves are referred to as <i>lordotic</i> , while at the thoracic and sacral regions <i>kyphotic</i> (Spine Universe [1]) . . . . .	4
2-2	Structure of an intervertebral disc. Image retrieved from the work of Raj et al. [2] . . . . .	4
2-3	Comparison between normal and herniated disc. (Mayfield Clinic [3]) . . . .	5
2-4	Representation of spinal stenosis compared with the normal spine. (Mayo Clinic[4]) . . . . .	6
2-5	Comparison between the normal coupling of two vertebrae and the five different grades of relative dislocation caused by spondylolisthesis [5]. . . . .	6
2-6	Graphical representation of the interbody fusion surgical treatment. This is an example of a surgery performed from the posterior side of the spine. (American Academy of Orthopaedic Surgeons [6]) . . . . .	7
2-7	Visual overview of the possible surgical techniques for lumbar interbody fusion. Image retrieved from the work of Mobbs et al. [7]. . . . .	8
2-8	Interspinous distraction with COFLEX device. (Paradigm Spine [8]) . . . . .	10
3-1	Cloward's technique for interbody fusion. Image retrieved from the work of Cloward [9]. . . . .	12
3-2	The original Bagby Basket on the left; the Bagby and Kuslich revised design for human spinal fusion on the right. Image retrieved from the work of Bagby et al. [10]. . . . .	12
3-3	Examples of interbody fusion devices. . . . .	13
3-4	Example of plating system. The system can allow both rigid and semi-rigid screw fixations, since it features fixed and variable angle screws. Image retrieved from Stryker [11]. . . . .	17

3-5	Subsidence case, comparing postoperative with 6-month lateral radiographs. Case retrieved from the work of Barsa et al. [12]. . . . .	18
3-6	Simplification of subsidence, defined as the sinking of the interbody fusion cage in the adjacent vertebrae. . . . .	18
5-1	A) Compression testing configuration to study the mechanical properties of interbody cages. B) Representative samples of the metal blocks used for testing, which need to match the geometrical shape of the cage. Images retrieved from the ASTM-F2207 standard [13]. . . . .	24
5-2	Subsidence test set-up. Image retrieved from ASTM-F2267 [13]. . . . .	25
5-3	Mechanical properties of porous titanium according to the study of Ahmadi et al.[14]. . . . .	27
5-4	Cervical (A) and lumbar (B) implants manufactured in porous titanium through selective laser melting. . . . .	28
5-5	Dimensions of the cervical (A) and lumbar (B) implants. . . . .	28
5-6	Polyurethane foam samples prepared for DIC and compression testing. . . . .	29
5-7	A) Set-up for the compression test to evaluate the stiffness of the cervical cages. B) Close-up of the cervical cage being compressed. . . . .	30
5-8	A) Set-up for the compression test to evaluate the stiffness of the lumbar cage. B) Close-up of the lumbar cage between the metal blocks for compression. . . . .	30
5-9	A) Set-up for subsidence testing and the DIC system. B) Close-ups of the implant-foam assemblies for subsidence testing. The top image shows the assembly with the cervical cage, while the bottom image is with the lumbar one. . . . .	32
6-1	A) Design of the cervical implant used for the biomechanical study. B) Simplified cervical implant used for the computational study with focus on the thickness of the solid frame. For both A and B, the parts in black are in solid titanium, while the gray regions are in porous titanium. . . . .	36
6-2	Representation of the three main parts of the simplified cage. On the left, the posterior solid shield; in the middle, the cage frame in solid titanium; on the right, the porous core. The images represent cage C20, thus the one with 20% of solid frame. . . . .	36
6-3	Figure A displays the model of a simplified cervical cage. The colours correspond to different material properties, with black being solid titanium, gray porous titanium and yellow the polyurethane foam. Image A displays the implant-block system. Image B showcases the top views of the three cages used for this investigation, to highlight the differences in frame thickness. C0 refers to 0%, C20 to 20%, and C40 to 40% of solid frame. . . . .	37
6-4	A) On the left, representation of the coupling between the reference points and the surfaces of the cage indicated by the red lines; on the right, the concentrated force is applied to the reference point on the top, and an encastre boundary condition to the bottom reference point. B) On the left, representation of the coupled reference points and the tie interaction at the implant-foam interface indicated by the red lines and the red circles respectively; on the right, depiction of the applied load and encastre for the model of the system. . . . .	39

6-5	Examples of two mesh sizes employed during the convergence study of the model. On the left, the mesh size is 1 mm, while it measures 0.6 mm in the model on the right. . . . .	40
7-1	A) Graphic comparison of the mean stiffness values $K_d$ of the cervical (left) and lumbar (right) implants, in the two porosities (P80, P70). B) Bar-plots displaying the mean stiffness values of the implant-foam systems, $K_s$ , on the left for the cervical cages and on the right for the lumbar cages. The graphs present combinations with both porosities (P80, P70) and substrate densities (G20, G15, G10). In both A and B, the error bars indicate the standard deviations. . . . .	42
7-2	Force-displacement curves for the cervical implant-foam systems. . . . .	44
7-3	Force-displacement curves for the lumbar implant-foam systems. . . . .	44
7-4	A) Force-displacement curves for the cervical cages on the left, and the lumbar cages on the right. Each graph displays three curves of the means and 95% confidence interval of the tests performed with the three foam densities (G20, G15, G10). The data represented is for the cage with 20% apparent density (P80). B) Bar-plots displaying subsidence at physiological loading (250 N for cervical and 280 N for lumbar implants) for all the foam grades and porosity combinations. The left graph refers to the experiments for the cervical implants, while the one of the right is for the lumbar implants. The error bars indicate the standard deviations. . . . .	45
7-5	Figure A shows the reference image, in which the displacement distribution along the load direction is zero throughout the system. Figure B shows a capture at 780N arbitrarily chosen to illustrate an example of the measured displacement distribution along the $y$ and $z$ axes (refer to Fig. 7-6 for the coordinate system). Three points on the top and bottom foams respectively are selected, as well as two points on the cage. . . . .	48
7-6	3D plot of the set-up showing the reference axes in the Vic3D post-processing software. . . . .	49
7-7	Application of extensometers to check differences in the change of length between the top foam-implant, and bottom foam-implant. The extensometers were aligned along the centre of the foams-cages for all experiments. . . .	50
7-8	A) Bar-plots displaying the stiffness of the cages for the all porosities (P70, P80, P90) and frame thickness (C0, C20, C40) combinations. B) From the top, stress and displacement distributions comparison with constant porosity P90 and variable frame thickness. From left to right, C0, C20 and C40. . .	53
7-9	A) Bar plot displaying the implant-substrate system stiffness using the models with 0% (C0), 20% (C20) and 40% (C40) solid frame with all combinations of porosities and foam grades. B) Example of the comparison of displacement distribution for the cages C0, C20 and C40, with constant porosity P90 and foam density G20. . . . .	54
7-10	Displacement distribution of the block surface interfacing with the implant. From left to right, the foam densities were G10, G15 and G20 for the simulations with constant porosity P90 and cage C0. . . . .	55
8-1	Contact angle in hydrophilic and hydrophobic surfaces. Image retrieved from [15]. . . . .	59

---

8-2	Comparison between healthy and osteoporotic bone. Image retrieved from [16]. . . . .	60
8-3	Cervical cages in $\text{Si}_3\text{N}_4$ used for the study by Suh et al. [17]. On the left, the cage with an empty core; on the right, the cage core is filled with load-bearing porous $\text{Si}_3\text{N}_4$ . . . . .	61
8-4	BMD of lumbar spine in a group of 105 women. Data is part of the work of Rigg's et al.[18] . . . . .	62
8-5	Trends of bone mass for female and with aging. Image retrieved from <i>Anatomy &amp; Physiology</i> by Young et al. [19] . . . . .	63

---

## List of Tables

3-1	Overview of the properties for the most commonly used materials for spinal devices. . . . .	14
5-1	Number of experiments performed. Five experiments were performed per each combination according to the standard [13]. . . . .	26
5-2	Closed cell polyurethane foam characteristics for testing subsidence [20]. . . . .	26
6-1	Material properties in the finite element models. . . . .	38
7-1	Stiffness for the cervical cages. . . . .	41
7-2	Stiffness for the lumbar cages. . . . .	41
7-3	Stiffness and yield load of the systems with the cervical cages. . . . .	43
7-4	Stiffness and yield load of the systems with the lumbar cages. . . . .	43
7-5	Stiffness of the polyurethane foams extracted from the systems with cervical cages. . . . .	46
7-6	Stiffness of the polyurethane foams extracted from the systems with lumbar cages. . . . .	46
7-7	Subsidence at 250 N for the cervical implants with different porosities (P80, P70) combined with substrates of three densities. . . . .	47
7-8	Subsidence at 280 N for the lumbar implants with different porosities (P80, P70) combined with substrates of three densities. . . . .	47
7-9	Average and SD of $E_0 - E_1$ at physiological loading, 280 N in percentage, over all the repetitions for the experiments post-processed with DIC. $E_0$ (Eq. 5-2) referred to the change of length between the top foam and the implant, while $E_1$ indicated the change of length between the bottom block and the implant. . . . .	49
7-10	Stiffness of the cage with all combinations of porosities (P70, P80, P90) and solid-to-porous ratios (FP, C0, C20, C40, FS). . . . .	50

7-11 Stiffness of the implant-substrate system using the cage with 0% solid titanium frame (C0) for all the foam densities and porosities (P70, P80, P90) combinations. . . . .	51
7-12 Stiffness of the implant-substrate system using the cage with 20% solid titanium frame (C20) for all the foam densities and porosities (P70, P80, P90) combinations. . . . .	51
7-13 Stiffness of the implant-substrate system using the cage with 40% solid titanium frame (C40) for all the foam densities and porosities (P70, P80, P90) combinations. . . . .	51
7-14 Subsidence as maximum displacement of the top surface of the block using the cage with 0% solid titanium frame (C0) for all the foam densities and porosities (P70, P80, P90) combinations. . . . .	52
7-15 Subsidence as maximum displacement of the top surface of the block using the cage with 20% solid titanium frame (C20) for all the foam densities and porosities (P70, P80, P90) combinations. . . . .	52
7-16 Subsidence as maximum displacement of the top surface of the block using the cage with 40% solid titanium frame (C40) for all the foam densities and porosities (P70, P80, P90) combinations. . . . .	52

---

# Acknowledgements

This work represents the peak of these years as a master's student at TU Delft, during which I had the great opportunity to improve and apply my engineering skills to the medical field, allowing me to follow my passion. The learning experiences went way beyond the books, extending to a continuous process of self-discovery and personal growth. This would not have been possible without the great people and brilliant minds that I got to meet in these years, through courses, group projects and the social initiatives carried out by TU Delft.

I am especially grateful for my supervisor, Prof. Jie Zhou, who has supported me in my pursuit of extra-curricular initiatives and supervised my work throughout the literature study and thesis project. His guidance helped me through the definition of the problem statement and research questions. I would like to thank him for providing timely precious feedback on the report and presentations, and for always pushing me to go beyond my limits, believing in my potential. I would also like to thank Mauricio Cruz Saldívar for granting me access to his Abaqus software, without which I would have not carried out a timely computational study, and for introducing me to scripting in Python for Abaqus .

I would like to thank Amber Implants for giving me the opportunity to gain hands-on experience in the field of medical devices. I would like to thank Mohammad Ahmadi for the weekly discussions during the literature study which helped me outlining the research proposal that defined my thesis, and for providing me with the interbody cages and the polyurethane foams to perform the mechanical tests. Furthermore I would like to thank Pim Pellikaan for the weekly technical meeting to present and discuss the progress of my research and for providing me with useful suggestions and feedback for the computational study. I would also like to thank Adriaan Blok, a graduating student of the Materials Science and Engineering department, for providing me with the information and contacts to arrange the biomechanical study carried out in the Aerospace Structures and Materials Lab, and for precious insights and reflections during the weekly technical meetings.

I would like to thank the staff at the Aerospace Structures and Materials Lab where I carried out the mechanical testings for my project. I would like to thank Berthil Grashof for providing the safety briefing to access the lab and instructions for the compression machine. Furthermore, I would like to thank Gertjan Mulder for the lecture for the use of the DIC equipment and for suggestions and knowledge to perform accurate testings.

I am infinitely grateful to my parents for all the great support throughout the academic years. My experiences abroad have showed me how blessed I am to have parents that trust and look up to all of my decisions. My confidence and independence is a consequence of such trust, and I will be forever grateful to them for it.

Finally, I would like to thank all of the friends and acquaintances made in these past years for making life great in the Netherlands.

Delft, University of Technology  
August 12, 2019

Victoria Bruno

"The practice of medicine is an art, not a trade, a calling not a business, a calling in which your heart will be exercised equally with your head"

— *Sir William Osler*



---

# Chapter 1

---

## Introduction

The interbody fusion device, or cage, is a spinal implant that aims to stabilize the motion of the vertebral segments between which it is inserted, as a surgical remedy to severe disc degeneration. Although different failure modes have been reported in clinical studies and in the FDA database [21][22][23], these are mainly single case reports. Interbody fusion is most likely to fail on a larger scale due to the occurrence of cage subsidence, migration or non-union between vertebrae. In the market research performed by an emerging medical device company [24], neurosurgeons worldwide appointed subsidence as the leading cause of interbody fusion failure. Subsidence consists of the sinking of the implant in the adjacent vertebrae. Therefore, the aim of the current work was to search for solutions to overcome this complication.

### 1-1 Scope

The literature study prior to the current work revealed that the condition of bone in terms of its mineral density is the most influential factor for subsidence occurrence when comparing it with implant material, size and shape [17][25][26]. Furthermore, the advancements in additive manufacturing and tissue engineering provided the potential of porous implants in the orthopedic field. The findings of the biomechanical and computational studies on the influence of bone mineral density (BMD) led to the reflections on the different degrees of subsidence over a range of bone mineral densities, with attention to the recent innovative porous solutions. Therefore, the present research focused on the biomechanical effects of cage porosity on the implant-bone system considering a range of bone densities, towards finding an optimal solution for patients with poor bone quality. The investigation was carried out through an experimental study according to an American Society for Testing and Material (ASTM) standard created specifically for interbody fusion devices.

## 1-2 Structure of the report

Chapter 2 provides the reader with background knowledge about the intervertebral disc, the diseases associated with its degeneration and the surgical treatments. In Chapter 3, the spine cage is introduced, and an outline of the different implant designs and mechanical issues is provided. After preparing the reader with sufficient background knowledge about the topic, the rationale of the thesis is explained in Chapter 4, where the reflections that led to the research question are presented. In the *Biomechanical Testing* chapter, information on materials, methods and standards used in the mechanical tests are extensively discussed. Chapter 6 describes the steps taken to perform an exploratory computational study to answer one of the research questions. Chapters 7 and 8 include the results and discussion of the outcomes. Finally, the closing chapters 9 and 10 are meant to draw conclusions about the findings and to propose future work.

---

## Chapter 2

---

# The Spine

This chapter provides some background knowledge about the anatomy of the spine, the disease associated with disc degeneration and surgical treatments. This serves as an introduction to the interbody fusion implant which will be discussed in the following chapter.

### 2-1 The intervertebral disc

#### 2-1-1 Anatomy and physiology

The human spine is composed of thirty-three vertebral bone segments, appertaining to five main regions, which, starting from the top, are: cervical, thoracic, lumbar and sacral and the coccyx, Fig. 2-1. A healthy spine features a natural curvature referred to as *lordosis*, which can be noticed in Fig. 2-1. Specifically, the curves in the cervical and lumbar regions are called *lordotic*, while in the thoracic and sacral regions are termed *kyphotic*. The intervertebral disc (IVD) is an anatomical structure located between each pair of vertebrae and functions as a shock absorber throughout the spine. The assembly of the IVD and the adjacent vertebrae with the adjoining ligaments represents the functional spinal unit (FSU), also called motion segment. The IVD is composed of three main parts: the nucleus pulposus (NP), the annulus fibrosus (AF) and the cartilaginous endplates (Fig. 2-2). The nucleus is a gelatinous mass concentrated in the centre of the vertebral body. Its gel-like structure is due to proteoglycans and water within a network of collagen type II and elastin fibers. Surrounding the NP there is the annulus fibrosus, which consists of concentric lamellae with collagen and elastin fibers. The endplates are made of hyaline cartilage and separate the nucleus and annulus from the adjacent vertebrae [2]. The osmotic properties are a result of the presence and peculiar composition of the NP which allows the disc to resist the compressive forces that the spine is subjected to.

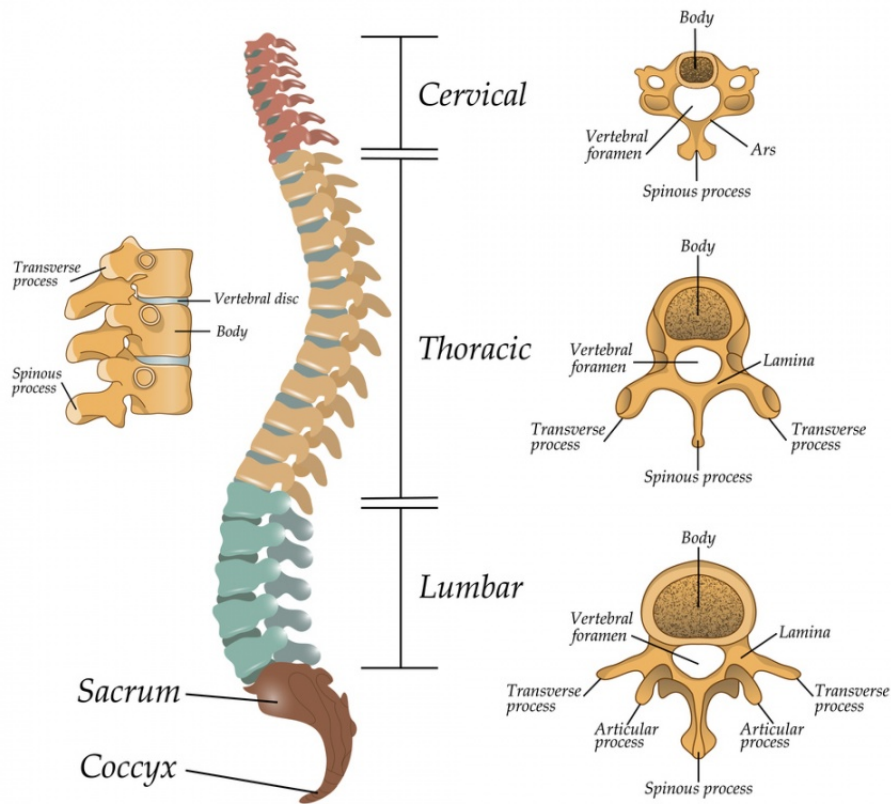


**Figure 2-1:** Representation of a human spine. The curvature of the overall spine is called *lordosis*. At the cervical and lumbar regions the curves are referred to as *lordotic*, while at the thoracic and sacral regions *kyphotic* (Spine Universe [1])

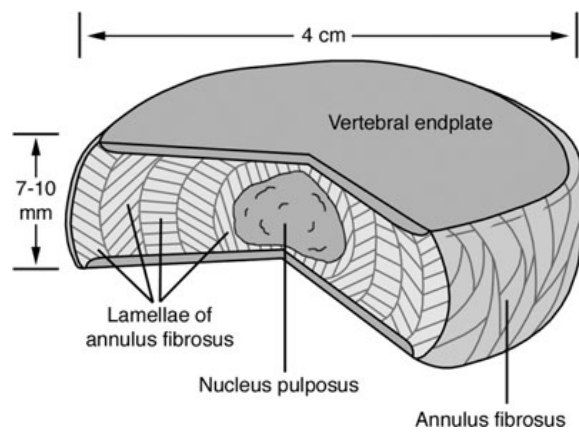


**Figure 2-2:** Structure of an intervertebral disc. Image retrieved from the work of Raj et al. [2]

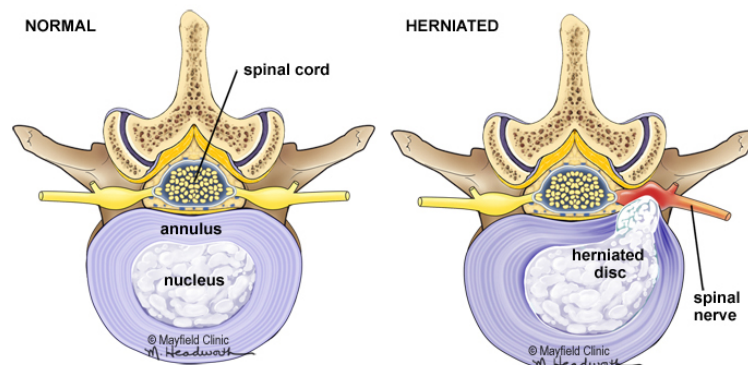


**Figure 2-3:** Comparison between normal and herniated disc. (Mayfield Clinic [3])

## 2-2 Pathophysiology and diseases

With aging, the IVD undergoes changes. Its overall structure progressively becomes disorganized, meaning the boundary between the NP and AF becomes less defined and the fibers networks start to appear scattered. The nucleus slowly loses its osmotic properties, becoming more fibrotic [27]. One of the reasons behind these gradual structural changes could be diminished blood supply to the intervertebral disc, which initiates tissue breakage [28]. Its degeneration can lead to low back pain (LBP) due to the instability of the vertebral joint, and sometimes can also develop into numbness and tingling sensations in the lower extremities [9]. The latter symptoms are commonly linked with disc herniation, which occurs when disc material is displaced, impinging the spinal nerves and causing their inflammation [9][29], Fig. 2-3. Specifically, sciatic pain has been associated with posterior disc bulges [30], which occur when the AF remains intact but presses against the nerves due to the penetration of the nucleus within it [31].

Other age-related diseases are spinal stenosis and spondylolisthesis. Stenosis is a condition where the spinal canal, nerve root canal, or intervertebral foramina narrow [32] 2-4. In spondylolisthesis, the vertebra displaces forward [33] and its severity is indicated by an assigned grade of 1 to 5 according to the amount of displacement (Fig. 2-5). Both of these diseases can be symptomatic of disc herniation, causing low back pain and leg pain if there is pressure on the nerves.

## 2-3 Surgical treatments

Treatments for low back and leg pain resulting from the mentioned diseases involve surgery whenever physiotherapy and pain killers are ineffective. Two techniques are worth mentioning, which are interbody fusion and interspinous distraction. The standard treatment is interbody fusion, but compared to the latter, it is an invasive procedure that involves the removal of portions of the vertebral bone to access the intervertebral space, thus weakening the neighbouring anatomical structures. Interspinous

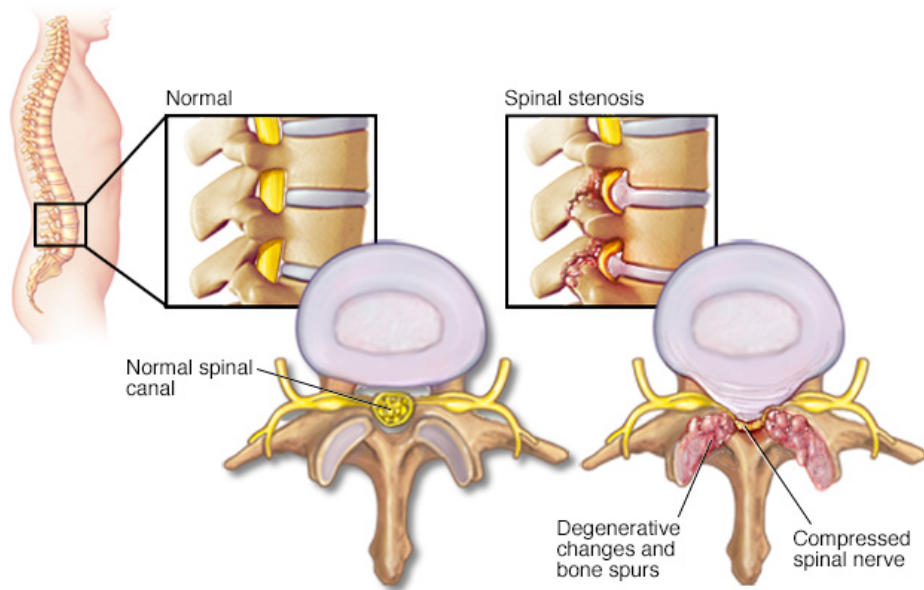


**Figure 2-4:** Representation of spinal stenosis compared with the normal spine. (Mayo Clinic[4])

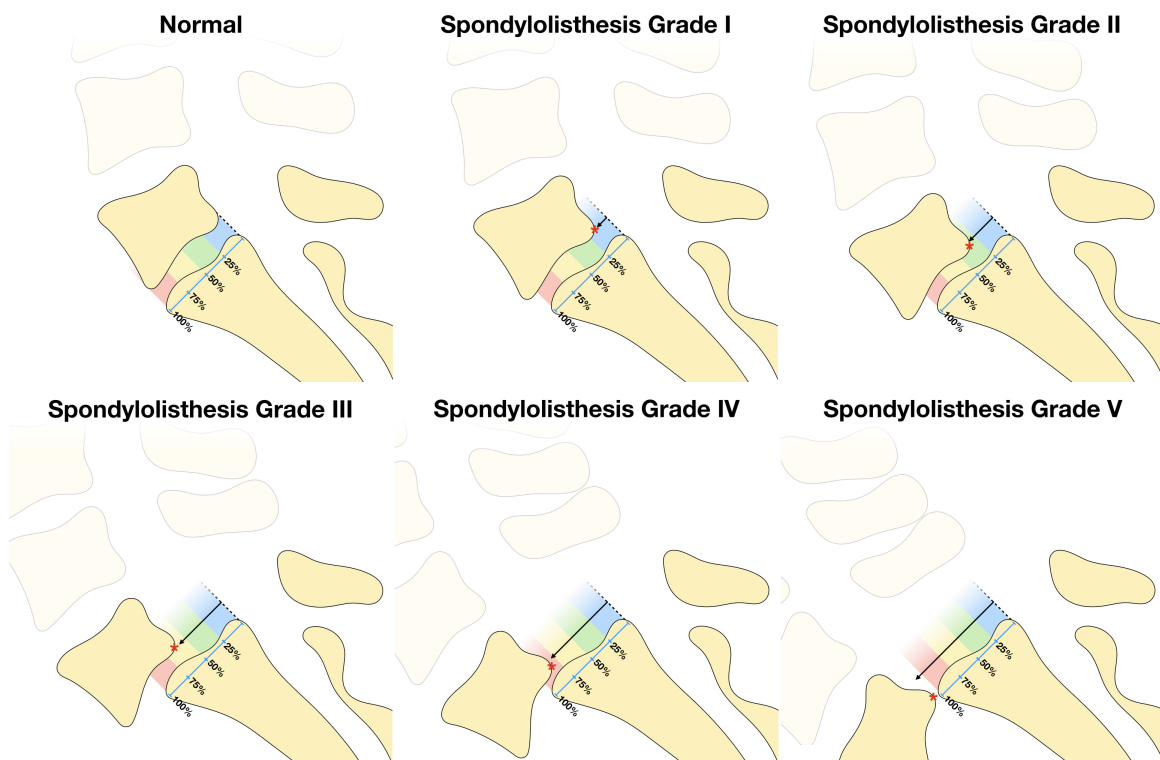


**Figure 2-5:** Comparison between the normal coupling of two vertebrae and the five different grades of relative dislocation caused by spondylolisthesis [5].

distraction is proposed as an alternative to limit these risks, and is mainly employed with the elderly [34].

### 2-3-1 Static stabilization: Interbody fusion

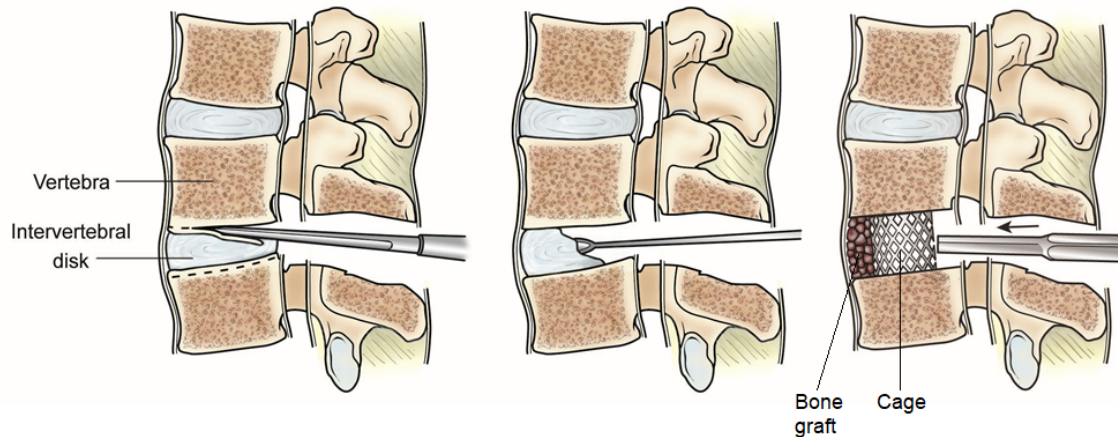


**Figure 2-6:** Graphical representation of the interbody fusion surgical treatment. This is an example of a surgery performed from the posterior side of the spine. (American Academy of Orthopaedic Surgeons [6])

Interbody fusion consists of the partial or total removal of the intervertebral disc followed by the insertion of an implant, also referred to as cage, in the disc space designed to allow fusion between the vertebrae. Through spinal fusion it is possible to eliminate the unstable motion of the FSU, while preserving the load-bearing function of the spine. Figure 2-6 displays the main steps of the surgical treatment. Firstly, muscle dissection or muscle-splitting is performed to reach the spine. Through a procedure called laminotomy, the lamina and spinous process, shown in the vertebrae in Fig. 2-1, are removed to achieve the decompression of the nerves and to expose the disc space. Then follows the retraction of the nerve roots to the side, which allows a corridor to the intervertebral space for the partial or total removal of the damaged disc and the endplate preparation [7]. The endplates are the parts of the vertebral body interfacing with the disc space, and their preparation consists of the partial removal of the cartilage of which they are composed to expose the underlying bleeding bone. This is necessary to trigger the bone growth within the cage that is inserted in the disc space, and it is of crucial importance for the success of the surgery that the endplates are still preserved to withstand the compressive forces of the inserted implant and bone grafts [35][36]. Interbody fusion nowadays can be achieved with various surgical techniques that differ in approach, grafting and cage materials, and fixation methods [37][38]. The insertion of the the spinal cage with grafts, besides stabilizing the FSU, restores the lost disc height and preserves lordosis, which is the natural curvature of the spine, as can be observed in the example of the healthy spine in Fig. 2-1. The implant used to achieve fusion will be further discussed in the next chapter.

Proietti et al. [39] have concluded that the decision-making for the surgical approach

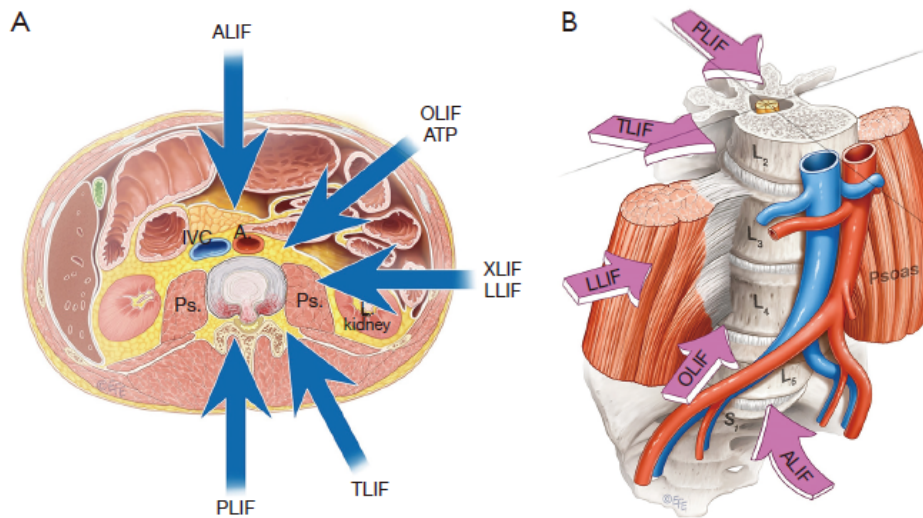


**Figure 2-7:** Visual overview of the possible surgical techniques for lumbar interbody fusion. Image retrieved from the work of Mobbs et al. [7].

should be done systematically and depends on many factors combined, such as age, disease, fusion levels and comorbidities. Furthermore, during this evaluation, it is important to estimate if these factors could lead to complications, such as an increased surgery time and amount of blood loss. One important decision to be taken concerns the use of fixation plates to further stabilize the segment. It is a crucial aspect since fixation plates have been associated with greater blood loss, risk of nerve injury or surgical time [40]. An increased re-operation rate has been observed, compared with the standalone cages [41][42]. Nevertheless, studies show that supplemental instrumentation may be necessary in some cases, such as primary degeneration [41]. The following sections will provide detailed descriptions of the available surgical methods, focusing on the lumbar procedures.

### Surgical techniques

All methods are divided into anterior and posterior approaches. The first group includes the anterior lumbar interbody fusion (ALIF) and lateral lumbar interbody fusion (LLIF) which are characterized by successful clinical outcomes at the cost of higher risk of injuries during the surgery and, specifically for ALIF, a higher incidence of cage migration [43]. On the other hand, the posterior lumbar interbody fusion (PLIF) and transforaminal lumbar interbody fusion (TLIF) require the surgeons to access the spine posteriorly through minimally invasive surgery due to the proximity of neural structures. Some cages may be designed for application of a specific approach. The following paragraphs briefly describe the most common surgical techniques, with reference to the specific operated levels shown in Fig.2-1.

**ALIF** The anterior lumbar interbody fusion procedure has been widely reported [43] and offers direct access for the implant insertion. It is mainly used to operate on the

levels L4/5 and L5/S1. It is not recommended for L2/3 and L3/4 since it is associated with anatomical limitations and higher risks [7]. This technique offers an advantageous view of the disc space, allowing better space clearance, endplate preparation and the possibility of inserting bigger interbody cages than with posterior approaches [44]. ALIF has been found to have better results when it comes to the restoration of disc height and lordosis, compared to TLIF and LLIF [43]. However, it requires peritoneal and vascular manipulation, making it an unfit approach for patients suffering from vascular, abdominal and spinal pathologies [45].

**LLIF** The lateral lumbar interbody fusion or extreme lateral interbody fusion (XLIF) refers to the techniques that access the spine laterally through the retroperitoneal fat and psoas major muscle [46]. Due to anatomical restriction from the iliac crest, it is not used for L5/S1. It can be advantageous for correcting aggressive deformities and the minimally invasive nature of the approach. Nevertheless, risks include psoas muscle, bowel or vascular injuries.

**PLIF** According to Mobbs et al. [7], the posterior lumbar interbody fusion approach is the second most used technique. The main advantage is that it offers good visualization of the nerve roots, thus favouring the surgeon's performance. Despite this, it is also associated with longer recovery time in case of muscle-trauma from the prolonged retraction [47]. It can be an inadequate technique when it comes to lordosis restoration, or more in general for endplate preparation. Compared with the TLIF approach, it has been reported to be more prone to complications and to take more time for the operation [25].

**TLIF** Lastly, the transforaminal lumbar interbody fusion was proposed to overcome the limitations of the PLIF approach. The neural foramen is opened only on one side, reducing the risk of damages that could be done to the anatomical structures of the spine. The risks associated with TLIF are the same as those for PLIF [48][49][47], with the difference that TLIF preserves ligamentous structures, keeping the segment more stable [50].

## Limitations

**Adjacent segment degeneration** Interbody fusion of a segment alters the loading and motion of the neighbouring vertebral joints. Adjacent segment degeneration (ASD) is a condition that may arise, and it is defined as the occurrence of radiographic alterations in the segments adjacent to the fused level [51]. These changes include accelerated disc degeneration, herniation and spinal stenosis among others [52]. It is believed the degeneration occurs as an effect of the altered biomechanical loading, which favours an increased intradiscal pressure and excessive loading of the facet joints [53]. ASD can further develop into a symptomatic disease which most often requires treatments through re-operation [51][54], such as decompression alone, decompression and fusion or decompression and disc arthroplasty [7]. Regrettably revision surgeries for interbody fusion are not very successful [54][7][53], therefore it is essential to investigate the different loading and displacements that the vertebrae are subjected to prior to and following the surgical treatment to optimize the interbody fusion.

**Lumbar non-union** The success of interbody fusion for the greatest part depends on bone healing. This process brings the vertebrae to fuse together and it is subjected to many different factors, such as the adopted surgical approach, the type of implant and bone graft, or the presence or absence of a fixation system [55]. Fusion can be defined as the bone formed between adjacent vertebrae of a segment through or around the inserted cages. It is usually assessed with radiographs from different perspectives taken post-operation, six, twelve or more months after surgery. Non-union, defined as the failed fusion between bones, may also occur and it could be caused by insufficient stabilization of the segment, poor surgical technique, trauma or infection. The occurrence of lumbar non-union has been reported to vary between 0% and 56% for lumbar fusion [56][57]. The assessment is done usually by surgeons that observe presence of bridging trabecular bone in radiographs.

### 2-3-2 Dynamic stabilization

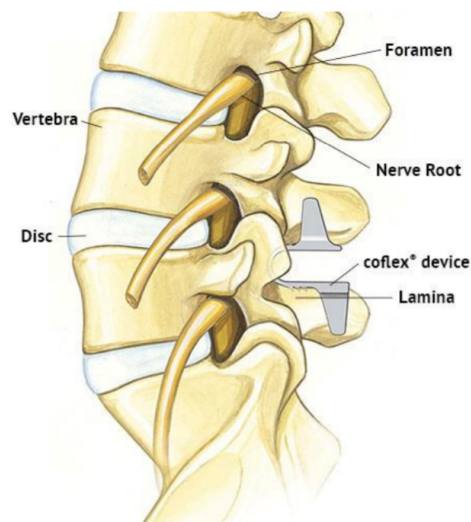


**Figure 2-8:** Interspinous distraction with COFLEX device. (Paradigm Spine [8])

**Interspinous distraction** Interspinous distraction, referred to also as dynamic stabilization, was introduced as an alternative to posterolateral fusion, Fig. 2-8. The main problematic linked to interbody fusion is the alteration of loading within the spine, which increases the biomechanical stresses acting on the adjacent vertebrae and, consequently, the risk of developing diseases at those levels [58]. Dynamic stabilization is a technique that overcomes this limitation by reducing motion and load transmission in the direction where pain is felt, rather than suppressing all motility of the segment [59]. The device designated for this approach is the intradiscal distractor, or interspinous process spacer, which functions as a shock absorber as it is placed to open the intervertebral foramina [60]. As an effect, the nerve roots are decompressed, the axial load is transferred to the anterior part of the disc, and the extension is limited [61], which may relieve pain [62]. Although less surgical complications are associated to this treatment, systematic reviews report a high incidence of revisions, thus being also costly.

# The Interbody Fusion Cage

In this chapter the interbody fusion implant, also denominated cage, is described. An overview of the technological improvements, main features and limitations are provided. The information in this chapter helps laying out a foundation to comprehend the problem statement and the research questions presented in the following chapter.

### 3-1 History

The original technique for interbody fusion was described by Cloward in 1952 [9], which consisted of the insertion of bone grafts harvested from the iliac crest of the patient into the hollowed disc space to trigger fusion, Fig. 3-1.

Although it was shown to be successful, this technique came with the great limitation of morbidity in the ilium. In 1988 Bagby introduced a device that improved Cloward's method by avoiding bone harvesting [63]. The idea was developed and studied on horses suffering from a syndrome comparable to spondylitic myelopathy, the Wobbler Syndrome, that caused neck instability. The first prototype consisted of a stainless steel cylinder with holes that allowed bone ingrowth, promoted by chips of cancellous bone packed inside the device, Fig.3-2. This so called "Bagby Basket" was proven to be efficacious and was later improved for human use by selecting different materials and physical features. It was approved by the U.S. Food and Drug Administration (FDA) in 1996 as the Bagby and Kuslich (BAK) Interbody Fusion System [10].

In the years followed, the surgical procedures developed into safer and less invasive techniques, and consequently the cage designs advanced with respect to the original concept. Fig. 3-3 presents examples of marketed interbody cages with their distinguishing features. It should be noted that the type of implant changes according to its site of destination, whether it is for the cervical or lumbar region of the spine. In general, the lumbar devices are more slender, longer and higher.

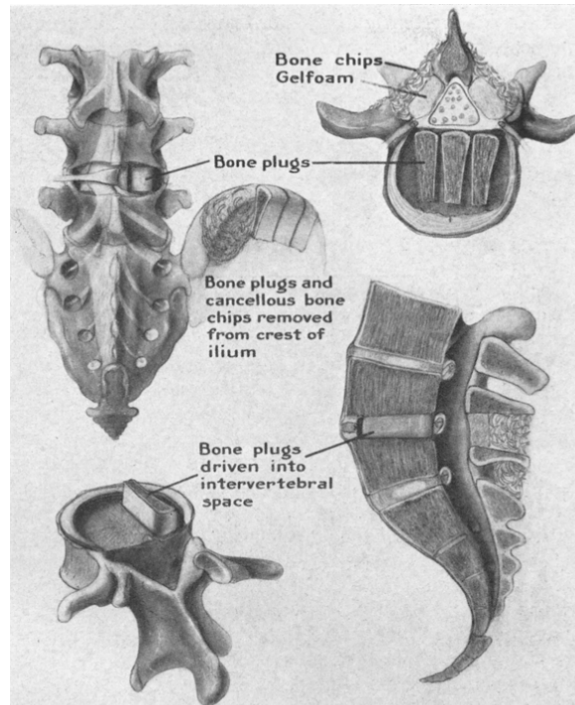


**Figure 3-1:** Cloward's technique for interbody fusion. Image retrieved from the work of Cloward [9].

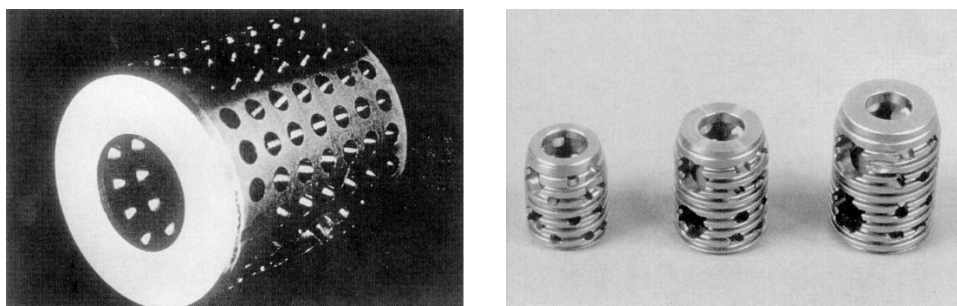


**Figure 3-2:** The original Bagby Basket on the left; the Bagby and Kuslich revised design for human spinal fusion on the right. Image retrieved from the work of Bagby et al. [10].

	Product	Supplier	Material	Type	Features
	CeSPACE® PEEK, Aesculap®	B. Braun	PEEK	Cervical, ACDF	-
	CeSPACE® Titanium, Aesculap®	B. Braun	Titanium	Cervical, ACDF	Plasmapore® coating
	Luna® Interbody Implant	Benvenue Medical	PEEK	Lumbar, ALIF	Expandable
	StaXx® XD Expandable Device	Spine Wave	PEEK	Lumbar, posterior	Expandable

**Figure 3-3:** Examples of interbody fusion devices.

## 3-2 Static and expandable cages

The gold standard to perform interbody fusion had been through the anterior part of the spine, before the posterior approach was introduced. The anterior technique is advantageous due to the wider corridor that makes the endplate preparation and the device insertion more practical. Its effectiveness is also related to the type of cage employed, which features a wide contact surface with the bone, compared to the devices used for the posterior approach [64]. Despite these favourable aspects, its great limitation is found to be the invasive nature of the surgery. As mentioned in Chapter 2, to overcome the morbidities associated with the anterior approach, surgeons developed a minimally invasive technique accessing posteriorly (PLIF, TLIF) through a narrower corridor. This meant that the cage had to be smaller for insertion, while fulfilling its functions of disc height restoration and segment stabilization. Vertically expandable cages were introduced, as opposed to the original static design, such as the Bagby Basket, Fig. 3-2. Two examples are provided in Fig. 3-3. The expandable design allows its insertion in the intervertebral space in a collapsed configuration, followed by its expansion in situ. This feature is advantageous compared to the static cage, since it offers the surgeon the option to optimize the fit according to the patient's anatomy [65]. The expandable device compared to the static, offers reduced nerve root retraction and impaction forces on the endplates in contact with the device [66][67]. Final cage height expansion is evaluated and selected by the surgeon and verified by intraoperative fluoroscopy. The procedure results in decreased blood loss, reduced muscle dissection and overall better post-operative recovery [68][69]. On the other hand, the use of

Property	Titanium	PEEK	CFRP
E modulus (GPa)	100-110	3.5	120-580
Radiodensity	Radiopaque	Radiolucent	Radiolucent
Promotion of osseointegration	Higher	Lower	Lower

**Table 3-1:** Overview of the properties for the most commonly used materials for spinal devices.

expandable devices is associated with an increased risk of the cage sinking into the vertebral body, being the main drawback when using expandable cages. These devices have a smaller contact surface, also referred to as footprint, and as a consequence higher stresses are observed at the bone-implant interface, which can lead to this undesired behaviour. A proposed solution is provided by the use of multidimensional expandable devices, which allows the expansion in the vertical direction as well as in the horizontal direction to increase the contact area.

### 3-3 Materials

#### 3-3-1 Titanium, PEEK and carbon fiber reinforced polymers

Another differentiating feature among cages concerns material. Three commonly employed materials for these implants are titanium, PEEK and carbon fibres reinforced polymers and an overview of their properties is available in Tab. 3-1. Titanium has been used for the longest in orthopedics, due to its resistance to corrosion, biocompatibility and the possibility to modify its surface roughness to increase cell adhesion [70]. The biocompatibility derives from the external oxide layer that forms when in contact with the fluids in the body [71]. The main issue regarding its application is the mismatch with the Young's modulus of bone, 100-110 GPa against 12 GPa for cortical bone, which leads "stress shielding". This phenomenon is initiated when specific bone cells, osteocytes, sense lower mechanical stress in the bone, due to the presence of the stiffer implant, which will bear greater load. According to Wolff's law, bone remodels depending on the mechanical stimuli on the bone, and reduced loading triggers bone resorption [72]. Moreover, fusion assessment is problematic due to its high radiodensity [73]. Instead, PEEK was introduced in the 1990s as a better option for what concerns stress shielding, thanks to its lower elastic modulus compared to titanium, and due to its chemical structure which grants it high resistance to chemical, thermal and post-irradiation degradation [74]. On the other hand, a systematic review of Kersten et al. [75] compared radiographic outcomes, and observed that PEEK is not necessarily a superior choice compared to titanium and carbon fiber cages [75], due to its lack of osseointegration and the formation of fibrous tissue around the cage. Furthermore, this material, being chemically inert, does not allow for protein absorption and promotion of cell adhesion [73]. Finally, there are cages, such as the Brantigan I/F cage for PLIF (DePuy AcroMed Corp., Raynham, MA), that are made of a carbon fiber reinforced polymers (CFRP) [76]. It has been found to be more reliable than allograft bone for what concerns fusion [77].

### 3-3-2 Porous titanium and osseointegration

The interbody fusion cages have seen a great transition, from smooth-solid surfaces with holes, such as the implants shown in Fig. 3-2, to the use of porous materials. This became possible thanks to the advancements in additive manufacturing (AM) which offers many advantages to orthopedic implants. AM enables greater use of metals for medical devices. For instance, because of its biocompatibility, titanium is a largely employed material in orthopedics. Nevertheless, its high stiffness compared to bone represents a limitation, since it causes stress shielding. AM technology allows the fabrication of porous metal with lower stiffness compared to the conventional manufacturing methods [78], thus expanding the possibilities for metal employment in orthopedics. This is possible by fine tuning the strut and pore sizes of metal lattices. The study by Chatham et al. [79] highlighted the advantage of the porous device as compared to non-porous ones, although in their study poly(para-phenylene) (PPP) was used, instead of titanium. By tuning strut and pore size, porous titanium could reach a Young's modulus of 0.6 GPa, and according to their work a Young's modulus of less than 1 GPa could reduce endplate stress, which translated to a lower risk of subsidence. Chatham et al. [79] compared four different lumbar spacers using PEEK, titanium, poly(para-phenylene) (PPP) and porous PPP (70% by volume). The results showed that the more compliant porous solution registered the lowest stress values at the endplates, reporting a stress of 0.431 MPa with the 70% porous PPP, against 0.473 MPa of the solid PPP spacer.

In addition, AM allows to produce highly customized lattices thanks to different manufacturing parameters that are easily controllable. An example is seen in selective laser melting (SLM), where optimization of laser power, manipulation of layer thickness and scan speed can significantly improve the mechanical properties of porous structures according to the end use [78]. The mechanical properties required for an implant may differ, depending on the site of implantation, because of the interactions with the surrounding cells and anatomical structures. Therefore, lattices can be designed as functionally graded materials (FGM), meaning that they vary in structural composition depending on their function, mimicking the behaviour of some tissues found in the body. A naturally graded material is the bone, composed of an outer shell of compact bone which encloses the less dense and more porous cancellous bone. This structure provides an example of biological adaptation to external loading and can help improve implant designs from a biomechanical perspective [80]. A critical aspect to determine the success of an orthopaedic implant is the achievement of osseointegration, defined as the linkage between the inserted device and the surrounding bone. As the knowledge of cell adhesion and proliferation grows, more attention is being given to the development of scaffolds that can help increase this process. When such bond lacks, a fibrous tissue around the device forms and triggers the resorption of bone, called osteolysis, in response to micromotion and inflammation, causing implant failure. An example is provided in the work of Gittens et al. [81], where the role of microstructures and nanostructures was analysed. It was well established that micro-roughness is beneficial for osseointegration, and its combination with nanostructures can further increase the positive effects [82]. In another study conducted by Garner et al. [83], an optimization algorithm was developed to achieve proper material connectivity when conceptualizing

lattices. When studying functionally graded materials, it is important that adjacent unit cells are compatible with each other at micro scale, in order to predict the behaviour at their boundaries and have a smooth transition of physical properties.

Finally, it is important to mention that in AM the products typically undergo a post-processing phase which includes surface treatments. Titanium, as mentioned earlier, is largely employed due to an oxide layer that forms externally in contact with the body fluid. This layer makes this material biocompatible, but at the same time it has low resistance to shear forces. To overcome this limitation, surface treatments are paired with the use of additive manufactured titanium to increase its resistance to wear and tear [71]. In general, there are many different types of surface treatments that can help improve a variety of material properties [71][84]. To mention one, chemical etching (CE) has been found to improve medical implants because it increases the osseointegration behaviour in titanium for instance [85]. It is a subtractive manufacturing process that consists of different phases in temperature regulated etching chemicals, and can substitute processes such as CNC and laser cutting for instance.

As opposed to AM, conventional manufacturing techniques involve casting and traditional metal powder processing methods, or machining in the case of titanium. To mention some disadvantages of these techniques, they are costly for the manufacturing of small series and for this reason with the advancements in AM, the orthopedic device industry is leaning towards new technologies. It is not possible to easily customize the devices and manufacturing time is much longer than that observed with 3D printing solutions. Furthermore, the conventional methods do not allow the creation of free-form structures that when included in prostheses, help accelerate the healing process in the body, such as in the case of cranial implant.

### 3-4 Stand-alone cages and plating systems

As mentioned in the previous chapter, the interbody fusion may require an additional fixation system. It is possible to differentiate between dynamic, semi-rigid and rigid systems. The first mentioned is not relevant for the current work, since it is used to alter the motion without the intention of fusion of the segment, as it is done in the already mentioned interspinous distraction. On the other hand, semi-rigid and rigid systems are employed to achieve stabilization, and consist of a system of screws and plates, as shown in Fig. 3-4. What differentiates these two systems is that in the semi-rigid system some relative motion between the pedicle screw and the plate is allowed, unlike the rigid system which achieves total fixation[86]. The rigid system can be advantageous to achieve rigidity and stabilization, on the other hand it has higher chances of causing stress shielding [87]. To avoid the invasive procedure of implanting the plating system, standalone devices are also commonly used, but a study highlighted higher incidence of subsidence in such cases [88].



**Figure 3-4:** Example of plating system. The system can allow both rigid and semi-rigid screw fixations, since it features fixed and variable angle screws. Image retrieved from Stryker [11].

## 3-5 Device limitations

### Cage migration and subsidence

Many complications are associated with the use of spine cages [39], but in this thesis the main focus was set on the failure linked to biomechanical performance of the device, specifically cage migration and subsidence. Cage migration refers to the displacement from the initial allocation in the intervertebral disc, specifically towards the posterior part of the vertebral body. The majority of clinical studies in the literature consider migration as a displacement greater than 3 mm [89][90][91][50], and the main cause of this phenomenon is indicated to be inadequate cage height. This is often seen when employing the PLIF approach, since appropriate distraction is hard to achieve. Lack of contact with the endplates could occur, resulting in non-union [92]. The migration has also been associated with the improper stabilization when posterior instrumentation is missing, which is usually the case for minimally invasive procedures to avoid surgical complications [93][94].

Subsidence is a specific case of migration and refers to the sinking of the device in the vertebral body, which also results in a decrease in disc height and loss in lumbar lordosis, Fig. 3-5. Clinical outcomes depend on subsidence, although in some cases this phenomenon can occur without presenting symptoms. It can lead to non-physiological loading and increased motion of the adjacent vertebral joints, resulting in faster degeneration [66]. In most clinical studies, subsidence has been defined as the sinking of more than 3 mm into the adjacent vertebrae [89][95][91][12]. Subsidence can exist in the overlying, underlying or both vertebrae, as can be seen in Fig. 3-6. Barsa et al. [12] evaluated some risk factors for the occurrence of this phenomenon. Over-distraction has been identified as one of the causes, together with the small contact area between implant and bone, and improper preparation of the endplates. Ideally, endplates should be preserved to prevent the implant from sinking, but in order to trigger vascular ingrowth within and around the implanted device, the surgical technique involves the removal of the cartilaginous tissue [96][90]. This lowers the mechanical condition of the bone, thus enhancing the risk of subsidence.

Many computational and biomechanical in the literature focus on the factors influencing subsidence by assessment of the stresses or displacement distribution at the implant-bone interface. In the computational study conducted by Chatham et al [79], the group besides comparing the stresses at the interface resulting from the variation of implant



**Figure 3-5:** Subsidence case, comparing postoperative with 6-month lateral radiographs. Case retrieved from the work of Barsa et al. [12].

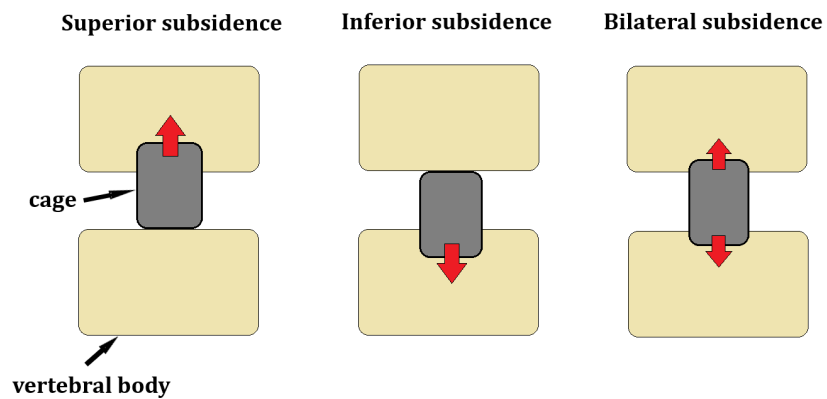


**Figure 3-6:** Simplification of subsidence, defined as the sinking of the interbody fusion cage in the adjacent vertebrae.

material, they analyzed the change in stresses when interchanging between a standard implant and a custom implant. The custom made cage had a larger footprint and that provided a 37-41% decrease in mean stress when compared to the original standard spacer, for each material. Increasing the device surface area for instance would be beneficial, but cannot be considered a feasible solution when designing a spinal cage, since there are restrictions dictated by its surgical insertion and anatomical features. This limitation was found to be the same as the study on shape optimization conducted by Hsu et al. [26], in which an algorithm developed to find the optimal shape according to total reaction forces revealed a flower shaped cage as the best solution. This showed the possibilities of the tool that was developed, but the output was not proved to be suitable for its purpose. The generated designs did not seem to consider surgical and anatomical limitations. Finally, a study conducted by Suh et al. [17] compared the influence of cage morphology, material composition and bone density on subsidence which helped understanding in which area to set the focus to improve the performance of the existing interbody cages. Interestingly, the study revealed the bone density as the most influential factor, by using polyurethane foam as a substrate material. Despite these outcomes, the clinical studies available in the literature do not provide results to validate the influence of bone density on cage subsidence, since in retrospective studies is common to find the percentages of patients in which the cage subsided without including and assessment of the condition of their bone.



# Thesis Rationale

The current chapter explains the rationale that led to the definition of the problem statement and the research question.

### 4-1 Overview

The literature study conducted prior to the current thesis work helped identify the condition of the underlying bone as the main factor for subsidence occurrence in patients undergoing interbody fusion [35][17][36][97][12]. Furthermore, the survey highlighted the advantages of employing porous implants, since they have the potential to overcome non-union, subsidence and cage migration through enhanced osseointegration [81] and stiffness reduction of the devices [79][98]. By reducing stiffness, the stresses at the bone-implant interface decrease, reducing the risk of subsidence and bone damage.

Additive manufacturing has significantly enhanced the possibilities for implant customization thanks to the lower manufacturing costs for small batches or single products, and the greater geometrical freedom in production compared to the conventional methods [99]. The issues related to the development of patient-specific implants are the longer planning time required prior to manufacturing [100][101], the need for highly specialized personnel, and expensive 3D printers needed to meet the precision requirements [102]. This project investigated a more feasible and cost effective method to offer tailor-made solutions, by setting the focus on the bone condition through the evaluation of bone mineral density (BMD). A specific product, such as the interbody fusion cage for the lumbar region, could offer a range of porosities that could lower the risk of subsidence. In fact, implants featuring higher porosity could potentially be beneficial to reduce the stiffness of the implant-bone systems, which translates to the decrease of the stresses at the interface, while increasing osseointegration. On the other hand, if an implant is too porous it could lack the strength to withstand the compressive loads in the spine and cause cage failure. In the literature, studies on porous implants are

increasing, although there is still a lack of clinical studies adopting the already marketed solutions. As a consequence, it is still not possible to quantify the improvements of the outcomes compared to the non-porous cages.

## 4-2 Problem statement and research questions

This project was intended to evaluate and quantify from a biomechanical perspective the degree of improvement of subsidence behaviour by tuning the porosity of the implants relatively to the patient's bone mineral density to open the investigation for a new customization approach. The problem statement leading to the research questions is hereby defined:

**To what extent can design parameters of interbody fusion cages help avoiding subsidence while taking into consideration the variability of bone mineral density in patients.**

The research questions that were formulated and answered for the current thesis work are the following:

1. Can the variation of cage porosity, in terms of apparent density, produce significant changes in the stiffness of the implant?
2. How much can the bone condition, in terms of bone mineral density, influence the extent of subsidence?
3. Can specific combinations of cage porosity and bone mineral density reduce the stiffness for the implant-bone system?
4. To what extent does the solid titanium outer frame found in the design of porous cages influence the stiffness of the implant?

To answer the first three questions, a biomechanical study was conducted using two variants of cage porosity and three variants of bone density by using three polyurethane foam densities, which are typically used materials to model cancellous bone in biomechanical testings. The last question was tackled through an exploratory computational study, using a simplified finite element model of the cervical cage-bone system. The parameter used to make evaluations on subsidence was the stiffness of the cages and the cage-bone systems, since it measures the resistance to deformation.

# Biomechanical Testing

This section opens with a brief description of the standards used as references to evaluate the mechanical performance of the interbody cages. Furthermore, the materials and methods used to perform the biomechanical tests are reported.

## 5-1 Standards for Interbody Fusion Devices

The medical device industry is heavily standardized and regulated. There are two test methods provided by the ASTM International (formerly the American Society for Testing and Materials) specifically for interbody fusion spine cages. These are the *ASTM-F2077 Test Methods for Intervertebral Body Devices* [103] and the *ASTM-F2267 Standard Test Method for Measuring Load Induced Subsidence of an Intervertebral Body Fusion Device Under Static Axial Compression*[13]. It is not mandatory to comply with the standards, but they are usually employed since they provide a method to perform tests in a controlled way, thus making it possible to compare outcomes. Furthermore, the process of approval by regulatory institutions for a new device can be accelerated by compliance to these testing methods. It should be noted that these standards are not performance tests, meaning that it is the manufacturer's responsibility to interpret the results and determine the device success or failure [104].

### 5-1-1 ASTM-F2077 Test Methods for Intervertebral Body Devices

This document provides methods to perform mechanical tests on the intervertebral body fusion device for either the lumbar, thoracic or cervical spine. It is not meant to directly predict the *in vivo* performance of the implants, but to collect information on the mechanical properties and compare the outcomes of different devices in a controlled way. The standard includes the methods for both dynamic and static testings, the former with the objective to evaluate the implant's risk of failure when exposed to

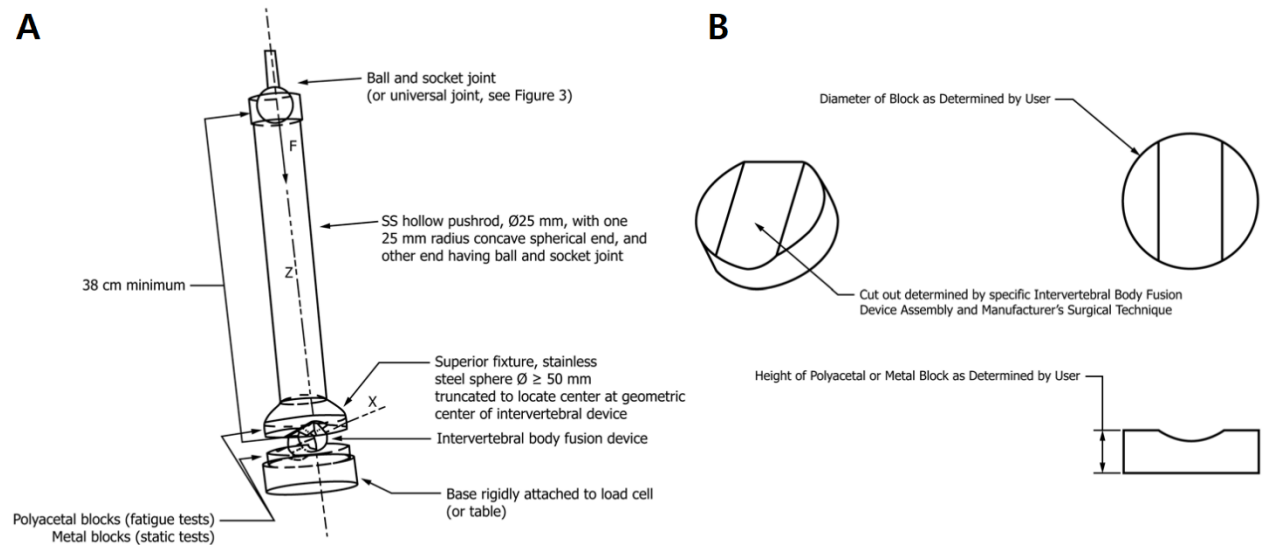


**Figure 5-1:** A) Compression testing configuration to study the mechanical properties of interbody cages. B) Representative samples of the metal blocks used for testing, which need to match the geometrical shape of the cage. Images retrieved from the ASTM-F2207 standard [13].

cycling loading, and the latter to characterize its mechanical properties [105]. Furthermore, information about three different types of test equipment are available, i.e. axial compression, compression-shear and torsion testing.

The set-up used for this project was for compression, as the one displayed in the drawing in Fig. A 5-1 provided in the standard [103]. Starting from the top, the set-up consisted of a hollow pushrod of 25 mm in diameter connected to the compression machine through a ball and socket joint. The pushrod had a concave spherical end to match the truncated sphere of the superior fixture, to allow a minimal sphere joint. The sphere had to be located at the geometric center of the cage. For the static tests, the implant had to be compressed between two stainless steel blocks, featuring cavities that matched the surfaces of the implant. These blocks had to be integrated to the superior and inferior fixture with screws through matching holes. This is evident in Fig. B 5-8.

### 5-1-2 ASTM-F2267 Standard Test Method for Measuring Load Induced Subsidence of an Intervertebral Body Fusion Device Under Static Axial Compression

This document provides a standard procedure to perform mechanical tests to evaluate load induced subsidence of the implant within polyurethane foam blocks. Unlike the ASTM-F2207, this standard only mentions static mechanical testing, specifically axial compression. The apparatus used to perform the test is the same as the axial compression configuration for the ASTM-F2077, Fig. 5-2, but using polyurethane foam blocks instead of metal, to mimic cancellous bone. Indications about the properties of the polyurethane foam blocks are also included, and the foam blocks have to conform to

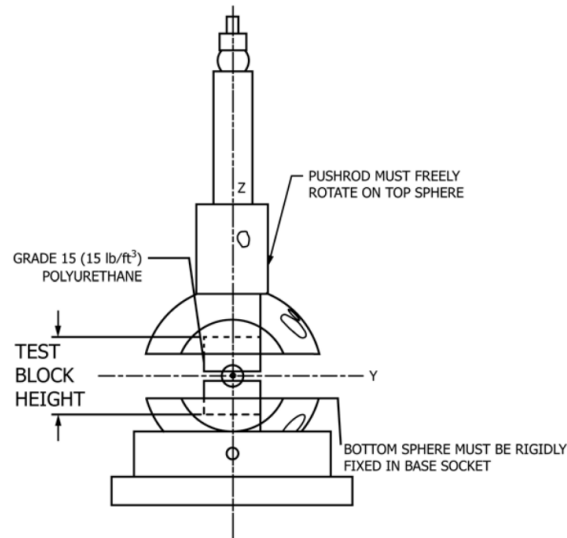


**Figure 5-2:** Subsidence test set-up. Image retrieved from ASTM-F2267 [13].

another standard which is the ASTM F1839. This document provides compositional, physical and mechanical requirements for polyurethane foams used in the testing of orthopaedic devices, and the foams are classified into ten grades. This material is widely used since it mimics the properties of cancellous bone, and the different grades provide a range of mechanical properties. Grade 15 foam is the one employed for testing load induced subsidence.

The first part of the test involves the characterization of the device stiffness  $K_d$  using axial compression between two rigid metallic blocks, as done in ASTM-F2207. The subsidence test follows, which is done by placing the device between polyurethane foams prepared to match the geometry of the cage, as it would be during the surgical procedure. Indications on the polyurethane foams are provided by F1839 [106]. The compression test is used to quantify the stiffness of the system foams-device  $K_s$ , from which it is possible to extract the stiffness of the polyurethane foams  $K_p$  with the following equation

$$K_p = \frac{K_s K_d}{K_d - K_s} \quad (5-1)$$

$K_p$  is used as an indicator of the propensity of a device to sink into the endplates of the vertebral bodies, and thus this value can be used to compare the cages with respect to subsidence. Higher  $K_p$  means a lower risk of subsidence of the cage into the adjacent vertebrae. The report of the test has to include the stiffness data, yield load and the description of failure. In the literature, research groups only include the subsidence comparison in terms of displacement [17][107].

	Cervical			Lumbar		
	G10	G15	G20	G10	G15	G20
P20	5	5	5	5	5	5
P30	5	5	5	5	5	5
Total	60					

**Table 5-1:** Number of experiments performed. Five experiments were performed per each combination according to the standard [13].

## 5-2 Test plan

### Interbody cages and test substrates

The purpose of the current work was to investigate the mechanical responses to two variables, i.e. the porosity of the implant in terms of its apparent density and the density of the polyurethane foam to model different bone conditions. The selected variables were combined for the lumbar and the cervical implants and are as follows:

- apparent density: 0.20 and 0.30 [14];
- grade: 10, 15 and 20 [106];

amounting to eighteen combinations for each type. The 0.20 apparent density corresponded to 80% porosity, while 0.30 corresponded to 70%, therefore they were referred to as P80 and P70 cages respectively. Grades 10, 15 and 20 corresponded to  $160.2 \text{ kg/m}^3$ ,  $240.3 \text{ kg/m}^3$  and  $320.4 \text{ kg/m}^3$ , respectively, with reference to standard ASTM-F1839 for rigid polyurethane foams as testing materials in biomechanical studies. These grades were selected to include a range of bone conditions, from osteoporotic (grade 10) to normal (grade 15) to denser than normal (grade 20). The implants were provided

Cellular Rigid Polyurethane Foam (Sawbones)				
Density		Volume Fraction	Cell Size (mm)	Compressive Modulus (MPa)
PCF	$\text{kg/m}^3$			
10	160.2	0.14	0.5-2	23.0
15	240.3	0.20	0.5-1.0	68.4
20	320.4	0.27	0.5-1.0	137.0

**Table 5-2:** Closed cell polyurethane foam characteristics for testing subsidence [20].

by Amber Implants B.V. They were manufactured through SLM of Ti6Al4V ELI, and were tested without applying any surface treatment. Figures A and B 5-4 display the cervical and lumbar implants respectively. The designs for both feature a frame in solid titanium and an inner porous lattice of diamond unit cell. The cervical implants had dimensions 12x14 mm for the footprint and 10 mm in height, while the lumbar implants were designed to have a footprint of 10x16 mm and height of 15 mm. Figures A and B 5-5 indicate the main dimensions of the cage designs.

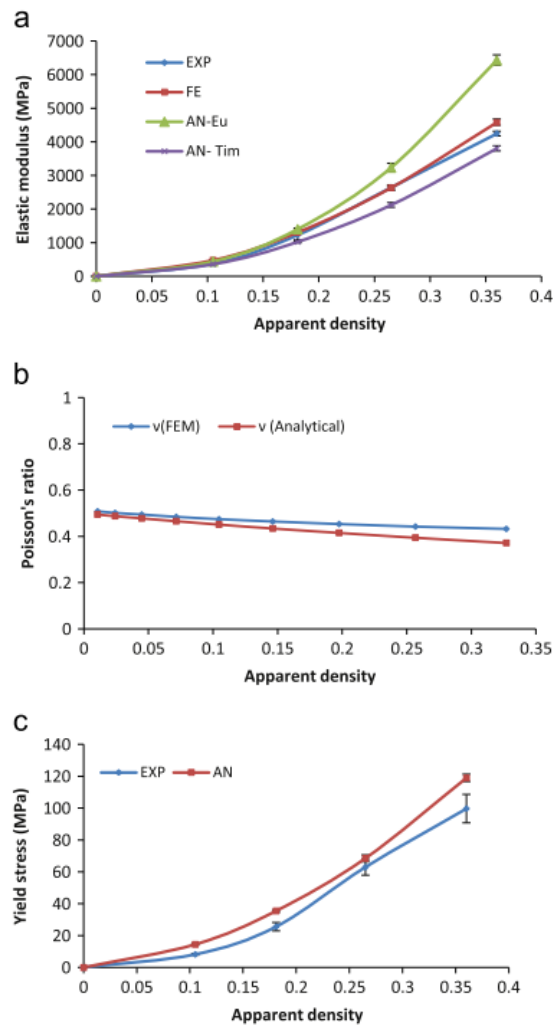
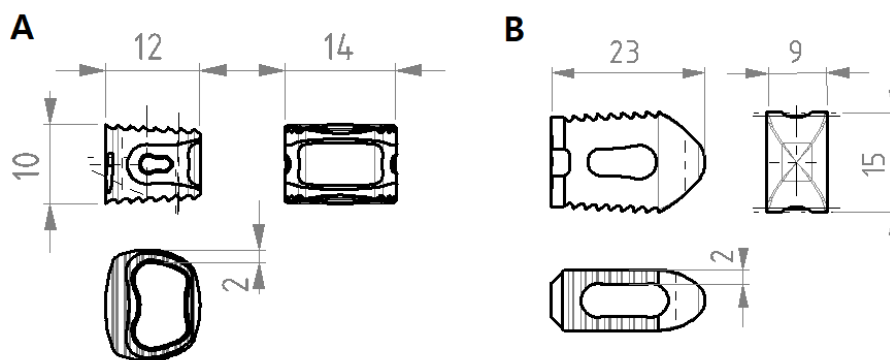


Figure 5-3: Mechanical properties of porous titanium according to the study of Ahmadi et al.[14].



**Figure 5-4:** Cervical (A) and lumbar (B) implants manufactured in porous titanium through selective laser melting.



**Figure 5-5:** Dimensions of the cervical (A) and lumbar (B) implants.

### 5-2-1 Sample preparation

The polyurethane foams (Sawbones; Pacific Research Laboratories, Inc.) were cut into 120 blocks to perform 60 experiments, 5 test samples per each test according to the standard [13]. Table 5-1 summarizes the combinations and the number of experiments performed. Since comparison of the offset yield displacements is included in the standard, it is stated that the foams could only be used once, while the cages could be retested, unless microscopic and geometrical evaluation revealed damage or permanent deformation. The dimension of the blocks for the cervical and lumbar experiments were respectively  $41 \times 37 \times 20 \text{ mm}$  and lumbar  $41 \times 43 \times 29 \text{ mm}$ , and these blocks were prepared to be tested along the direction of rise, which was indicated in the certificate of compliance distributed by Sawbones. The direction of rise refers to the technique used to manufacture these foams, through polymerization in free-rising [108] which can cause anisotropic properties to the foam [109]. ASTM-F2267 includes indications for test block height, referenced in Fig. 5-2, which should be  $70 \text{ mm}$  and  $40 \text{ mm}$  for test-



**Figure 5-6:** Polyurethane foam samples prepared for DIC and compression testing.

ing lumbar and cervical implants respectively. The distance depended on the heights of the implants, therefore being 15 mm for the lumbar implant and 27.5 mm for the foam. The cervical cage height was 10 mm, meaning the foam needed to be about 15 mm. The final dimensions were slightly larger within an error tolerance of 1.5 mm. The foams were then painted and speckled to perform digital image correlation (DIC), labelled and marked to reference the centre to allocate the implant. The end results are shown in Fig. 5-6.

### 5-3 Test set-up

Two compression tests featuring different testing conditions were performed according to the standard ASTM F2267. The first consisted of the measurement of the stiffness of the titanium implants, using the metal blocks, while the second part was done to measure subsidence within the polyurethane foam blocks.

#### 5-3-1 Compression test for implant stiffness

The components of the set-up for the compression test was provided by Amber Implants B.V. [24], with the exception of the metal blocks to match the outer shape of the cervical implants. Therefore two different set-ups were employed for the cervical and lumbar implants, the latter not complying to the ASTM F2207.

The compression tests for the cervical implants were performed with the Zwick Z100 tensile/compression machine. Two metal plates were placed between the cage and the fixtures. Furthermore both fixtures used allowed the accommodation of an angle of 3° to match the surface of the cage. The strain rate applied was of 1.8 mm/min, the end of test was set to 25 kN and the applied preload was 200 N, as indicated in the standard [103].

The machine used to measure the stiffness of the lumbar cages between the metal blocks

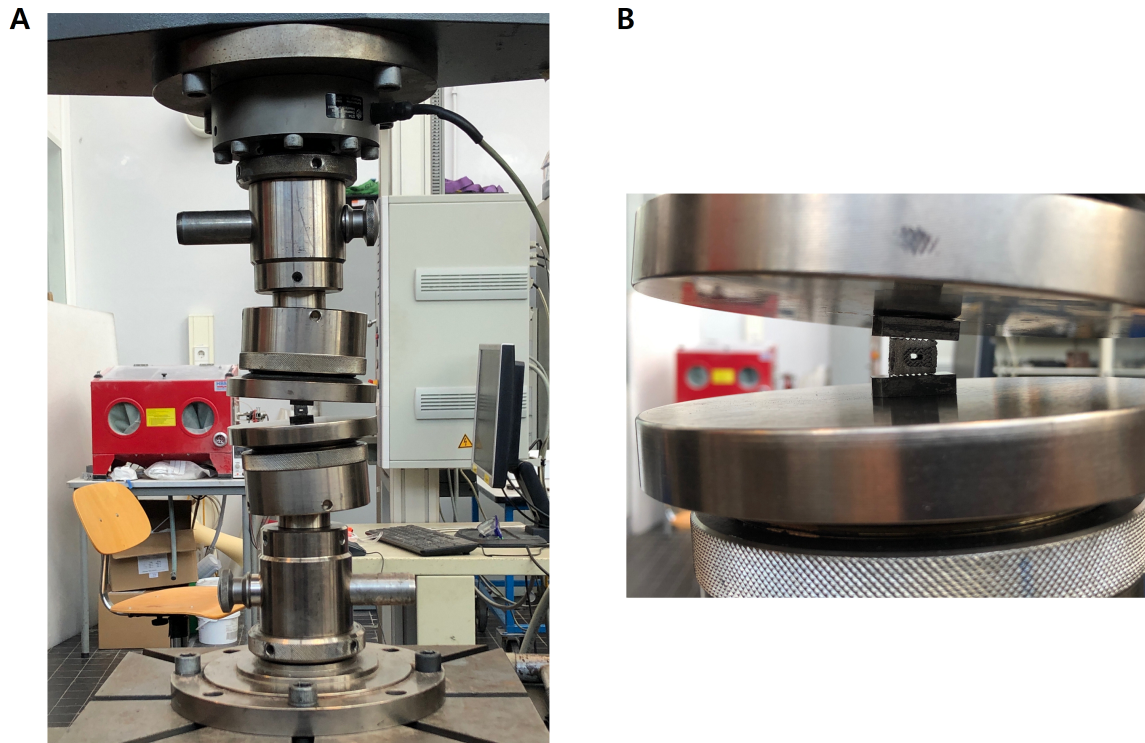


**Figure 5-7:** A) Set-up for the compression test to evaluate the stiffness of the cervical cages. B) Close-up of the cervical cage being compressed.

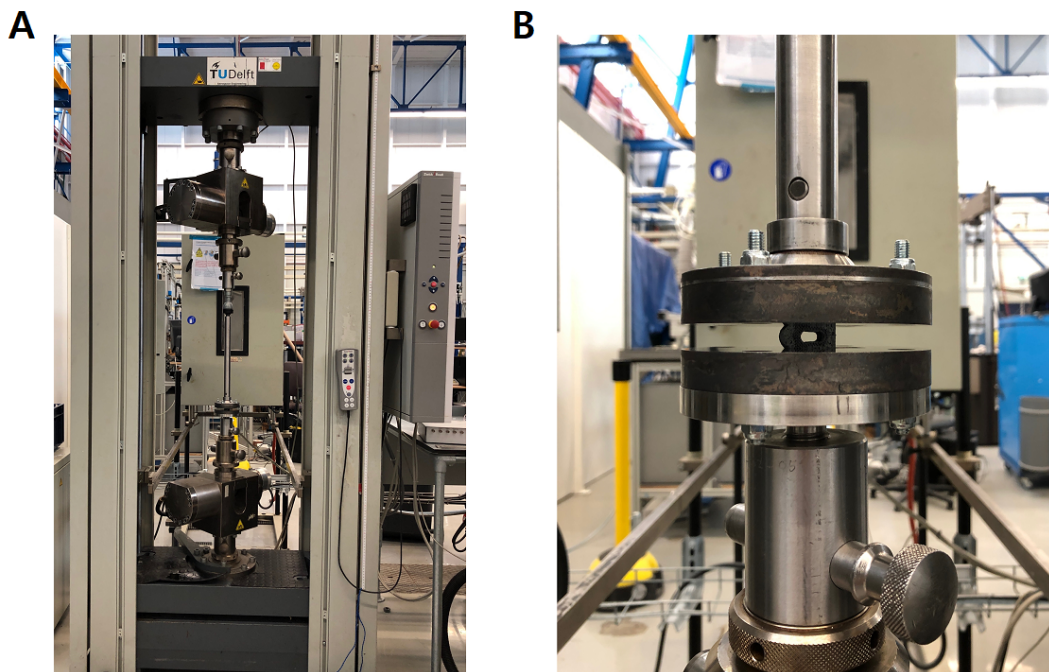


**Figure 5-8:** A) Set-up for the compression test to evaluate the stiffness of the lumbar cage. B) Close-up of the lumbar cage between the metal blocks for compression.

was a Zwick 250 kN tensile/compression testing machine and the set-up was according to the standard F2267, Fig. 5-8. The end of test had to be set to 25 kN while a preload of 500 N was applied. The compression rate was set to 1.8 mm/min within the range suggested in ASTM F2207. The setup to test the cervical cages was different from the suggested one in the ASTM F2207 due to the lack of metal blocks matching the cage geometry, Fig. 5-7. The compression machine was Zwick 100 kN, and the preload and compression rate were set respectively to 100 N and 1.8 mm/min.

### 5-3-2 Compression test for subsidence

For the subsidence test a compression machine with a lower load cell, of 10 kN, was used to obtain more accurate results since the loading conditions were much lower compared to the compression tests for the stiffness of the cages. The machine used was the Zwick 10 kN tensile/compression test machine, the rate of compression was 6 mm/min and the end of test was set to a 5 mm displacement and/or 2250 N. The force value was chosen through prior testing on trial samples to verify that the yield point would be reached, since according to standard, the yield load had to be reported. It was previously used in another study in the literature [107]. Furthermore, clinical studies reported subsidence behaviour whenever the sinking of the cage was greater than 3 mm. Therefore, setting 5 mm implied subsidence within an acceptable displacement range, assuming subsidence would occur symmetrically in the adjacent vertebrae.

### 5-3-3 Subsidence measurement

The crosshead displacement was assumed to correspond to the overall subsidence, occurring in the superior and inferior foam blocks. Subsidence was compared at the physiological loading values found in the literature [17][98]. Specifically, for the cervical cages subsidence was measured at 250 N, and for the lumbar cages at 280 N, which are both higher than the actual loading in the body to allow a factor of safety. The human head generates a load of 50 N on the cervical spine, and the failure loads at the implant-endplate interface were reported to range between 754 and 2238 N [17][110]. The load for the lumbar cage is higher due to the additional weight coming from half of the body. The selected load included a factor of safety of 4 and was used in previous studies found in the literature [98][111]. Furthermore, the DIC system allowed to verify that the sinking of the cage within the foams occurred symmetrically up under the physiological loading. This means that the subsidence values registered corresponded to half of displacement within each foam block.

## 5-4 Statistical Analysis

The data collected by the compression machine and the DIC system were extracted and analyzed with a custom script for MATLAB and Excel. The number of samples

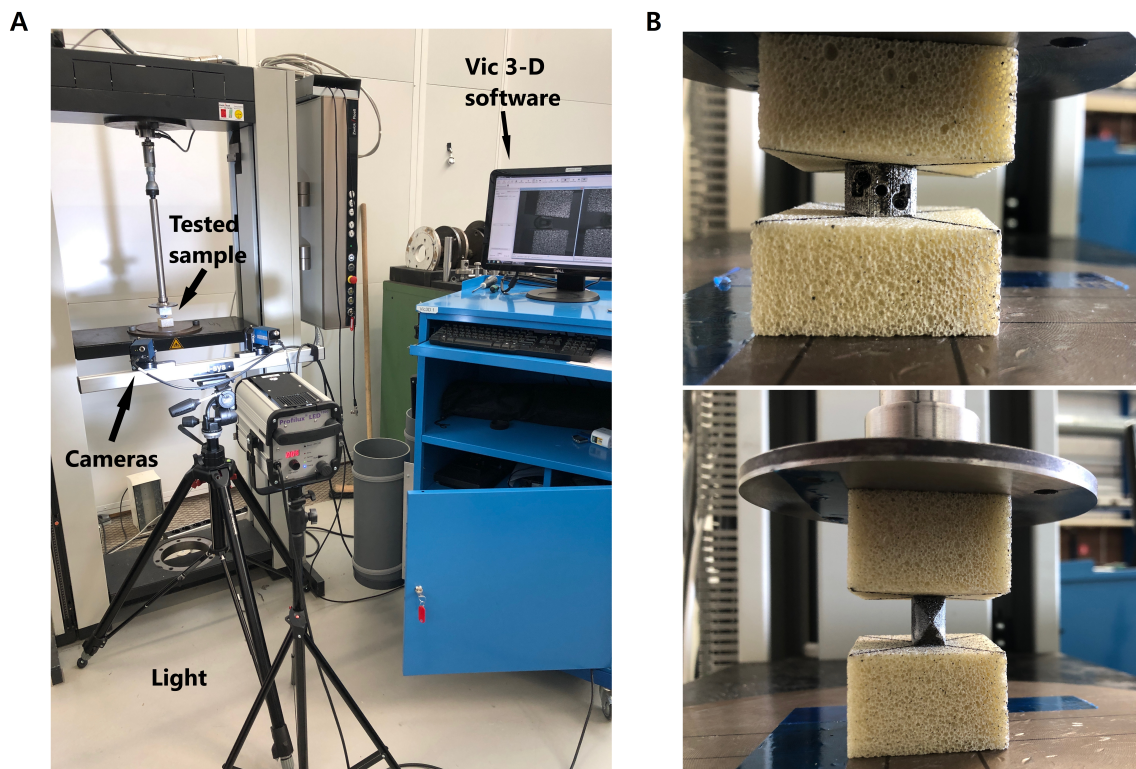


**Figure 5-9:** A) Set-up for subsidence testing and the DIC system. B) Close-ups of the implant-foam assemblies for subsidence testing. The top image shows the assembly with the cervical cage, while the bottom image is with the lumbar one.

per each experiment amounted to five, as suggested in the standard, and the statistical method employed was the two-way ANOVA in order to assess the effects of the porosity and the foam density independently, as well as their interaction with each other. When comparing only one parameter, the stiffness of the cages varied with to porosity, a t-test was performed. The level of significance in difference was defined as  $p < 0.05$ .

## 5-5 Digital Image Correlation System

The DIC system adopted in the current study was the VIC-3D 8 System (Correlated Solution, Inc.; Irmo, US). Two cameras of 4 MP were placed approximately at a 30° angle, put into focus and properly set through Vic-Snap software for visualization and calibration. The DIC set-up is shown in Fig. 5-9.

The data collected was later processed with Vic-3D post-processing software. The first step was the upload of the calibration images for recognition of the cameras allocations. After analysis of the data, the software was used to evaluate whether the subsidence was occurring symmetrically throughout the compression. In the current work, the focus was set specifically on the sinking of the cage within the foams until the physiological load. By verifying the symmetry of the phenomenon, it was possible to demonstrate that the measured crosshead displacement was equal to half the subsidence in each foam block. Furthermore, it allowed to extract a value of tolerance of the order of microns for any difference between the measured subsidence in the top and bottom foams. This was done by applying two extensometers from the option tools of the software, from the cage to the top and bottom foams, to extract the change in length in percentage and track any significant differences. The extensometers measured the change in length as

$$E = \frac{\Delta L}{L_0} \quad (5-2)$$

where  $L_0$  is the original length corresponding to the first image set as a reference,  $\Delta L = L_{@280} - L_0$ , and  $L_{@280}$  is the final length measured at the physiological loading of 280 N.



---

## Chapter 6

---

# Computational Study

This chapter opens with the scope of the computational study, which serve as a brief explanation and introduction for the materials and methods hereby described.

### 6-1 Scope

Titanium is largely employed as a biomaterial for biomedical applications, and more so for orthopaedic implants [112], which imply contact with bone. The main drawback for these applications is the stress-shielding effect, caused by the difference in Young's modulus between titanium implant and bone, resulting in bone absorption. The solid titanium, specifically Ti6Al4V- ELI for this study, is characterized by a Young's modulus of 110 GPa, while porous titanium can see its Young's modulus decrease a couple of orders of magnitude, ranging between 1-4 GPa [113]. The introduction of porous titanium opened new possibilities for surgical orthopaedics, although it cannot fully replace solid titanium to withstand the physiological loads, such as the compressive forces in the spine.

The computational part of the project served as an exploratory study to understand the influence of the thickness of the cage frame. The biomechanical study was thought to reveal differences in stiffness when changing the cage porosity. Since the implant was designed to have an outer frame in solid titanium, which had constant material properties when varying the porosity of the porous regions, an investigation on the influence of the solid-to-porous ratio was included. The design variables for the cage were numerous, therefore a computational study was used for a preliminary evaluation of the solid-to-porous ratio of the frame thickness of the cage.

In this chapter, the finite element models developed for the computational study are described. The three finite element models differed in the solid-to-porous titanium ratios of the cages to explore the degree of influence of the frame in solid titanium when analyzing the stiffness of both the cage and the cage-foam system. It was important to keep the cage geometry unvaried between the models, since the cage contact

surface, i.e. cage footprint, was demonstrated to influence subsidence [17] and since stiffness is dependent on physical dimensions. Moreover, the stiffness was evaluated for all porosities and foam densities, including the two extreme cases of fully porous and solid cages.

## 6-2 Geometries and material properties

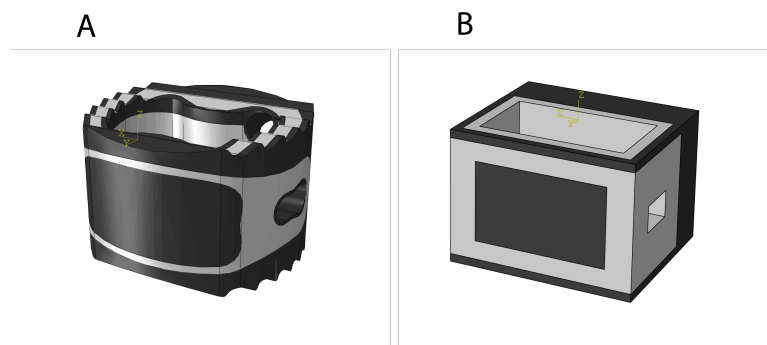


**Figure 6-1:** A) Design of the cervical implant used for the biomechanical study. B) Simplified cervical implant used for the computational study with focus on the thickness of the solid frame. For both A and B, the parts in black are in solid titanium, while the gray regions are in porous titanium.

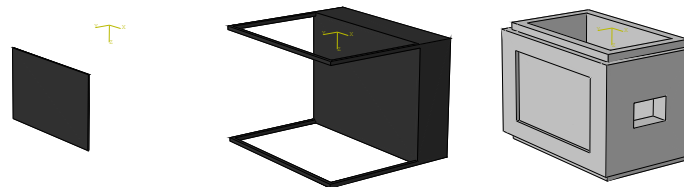


**Figure 6-2:** Representation of the three main parts of the simplified cage. On the left, the posterior solid shield; in the middle, the cage frame in solid titanium; on the right, the porous core. The images represent cage C20, thus the one with 20% of solid frame.

Three models comprising of the implant-block assembly were developed using the finite element analysis (FEA) software Abaqus. The cage was simplified, maintaining the main features of the real case, such as the central and lateral apertures, but most importantly respecting the differentiation between porous and solid titanium parts throughout the cage. The main dimensions were kept unvaried, being  $12 \times 14 \text{ mm}$  and height of  $10 \text{ mm}$ . The cage contact area measured  $100.9 \text{ mm}^2$  taking into account the central hole, and was kept constant between the three models to make sure that the

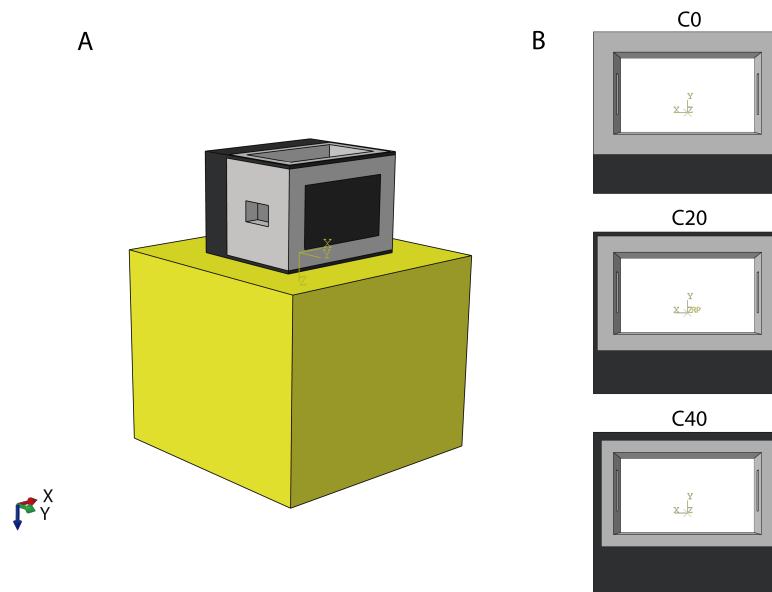


**Figure 6-3:** Figure A displays the model of a simplified cervical cage. The colours correspond to different material properties, with black being solid titanium, gray porous titanium and yellow the polyurethane foam. Image A displays the implant-block system. Image B showcases the top views of the three cages used for this investigation, to highlight the differences in frame thickness. C0 refers to 0%, C20 to 20%, and C40 to 40% of solid frame.

changes of stiffness would not depend upon geometrical changes, but solely upon the different material distribution. The frame of the cage measured  $1.5\text{ mm}$ , of which the solid titanium occupied 0% in the first model, 20% in the second model, and 40% in the third model (Fig. 6-3). From this chapter onwards the models will be referred to as C0, C20 and the C40 for simplicity. The parts comprising the cage were three: the solid frame, the porous core and an posterior solid shield, as shown in Fig. 6-2. The porous regions were modelled using the material properties according to the work of Ahmadi et al. [14], as opposed to the elaboration of a geometrical lattice. The porosities used for the computational investigation were the ones used for the biomechanical tests, P70 and P80, with the addition of a third more porous case P90. Moreover, the foam block was reduced in size compared to the real block used for the biomechanical test, to measure  $24 \times 24\text{ mm}$ , but leaving the height of  $20\text{ mm}$  unvaried. This was done to reduce the computational time, and was acceptable since the model was not used for validation purposes and the compression tests revealed no strain variations throughout the foam. The implementation of the material properties of bone for the block was considered, but was ultimately built using the same properties of the polyurethane foams to allow the validation of the biomechanical tests in future steps. The material properties were simplified to be linear elastic and are all reported in Tab. 6-1.

Components		Young's modulus (MPa)	Poisson's ratio	Reference
Foam block	G10	23.0	0.2	[20][109]
	G15	68.4	0.2	Sawbones
	G20	137.0	0.2	
Porous titanium	P90	406.9	0.47	
	P80	1577.5	0.45	Ahmadi et al. [14]
	P70	3328.4	0.43	
Solid titanium		110000	0.34	Niinomi et al. [112]

**Table 6-1:** Material properties in the finite element models.

## 6-3 Interaction properties and boundary conditions

### 6-3-1 Stiffness of the implant

For the evaluation of the stiffness of the cages for all the material combinations, the C0, C20 and C40 models were analyzed without the block. The bottom reference point was coupled directly to the bottom of the cage and fully constrained. Furthermore, a concentrated force of 15 kN, which had to be lower than the yield load observed in the mechanical tests, was applied the top reference point coupled with the top surface of the cage. The reference points were used to extract the force-displacement data to compute the stiffness of the cage.

### 6-3-2 Stiffness of the implant-block system

The model was composed of the foam block and the different parts constituting the simplified cage. The implant-block interface was modelled with a tie contact. The only force in the simulation was normal to all parts, therefore it was not necessary to include friction due to the absence of tangential components. Furthermore, two reference points at the top and at the bottom of the implant-block assembly were included and coupled respectively to the top surfaces of the cage and the bottom surface of the foam, as shown in Fig. 6-3. The reference points were used to apply the boundary conditions and to extract the data for force-displacement data to compute the stiffness of the implant-block system. The bottom point was fully constrained, while a concentrated force of 280 N was assigned to the top reference point (Fig. 6-4). The force magnitude was selected to stay within the linear region of the force-displacement graphs in accordance with the experimental study carried out in this study.

## 6-4 Mesh

Quadratic tetrahedral elements C3D10 were employed for the finite element models. A convergence study was conducted for the models used to assess the influence of the frame thickness by applying a concentrated force of 100 N to the top surfaces of the cage

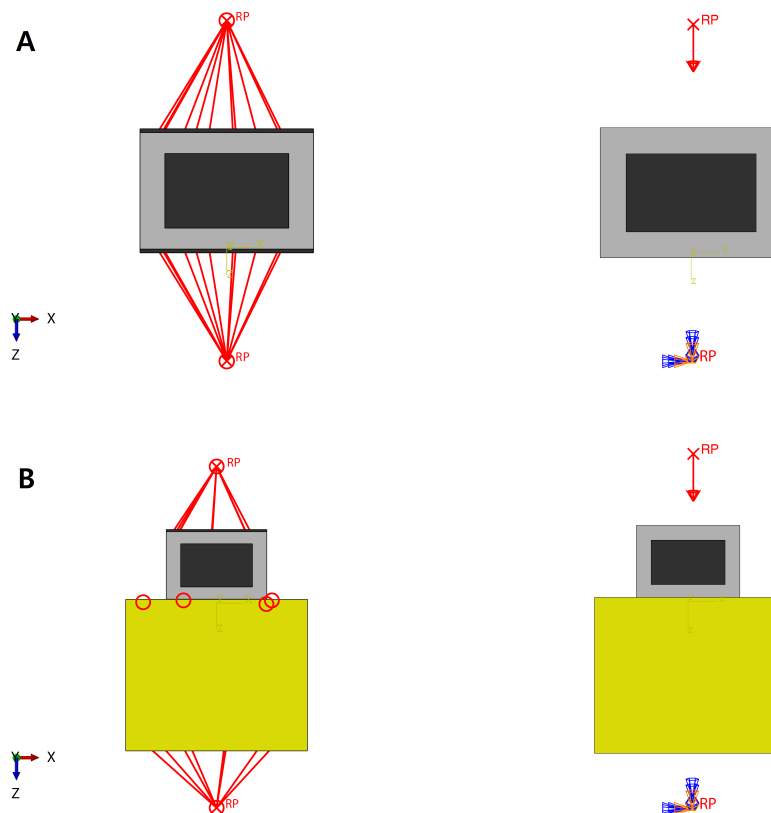


**Figure 6-4:** A) On the left, representation of the coupling between the reference points and the surfaces of the cage indicated by the red lines; on the right, the concentrated force is applied to the reference point on the top, and an encastre boundary condition to the bottom reference point. B) On the left, representation of the coupled reference points and the tie interaction at the implant-foam interface indicated by the red lines and the red circles respectively; on the right, depiction of the applied load and encastre for the model of the system.

and comparing the maximum displacement values. The number of elements employed in the selected mesh amounted to 224924 for C0, 227782 for C20, and 227225 for C40.

## 6-5 Limitations and assumptions

The goal of the computational study was to understand and explain the results obtained in the experimental study. For this reason a simplified cage was designed instead of the real implant to make it computationally efficient and verify the hypothesis. In the simplification, the draft angle of  $3^\circ$  for the cage and the matching foam was neglected. By assuming a zero draft angle, the tangential forces were assumed to be zero. The top and bottom surfaces were designed without the teeth displayed in the real implant, simplifying the contact problem. All material properties were assumed to be linear elastic, although in reality the foam blocks display a viscoelastic behaviour. The loads

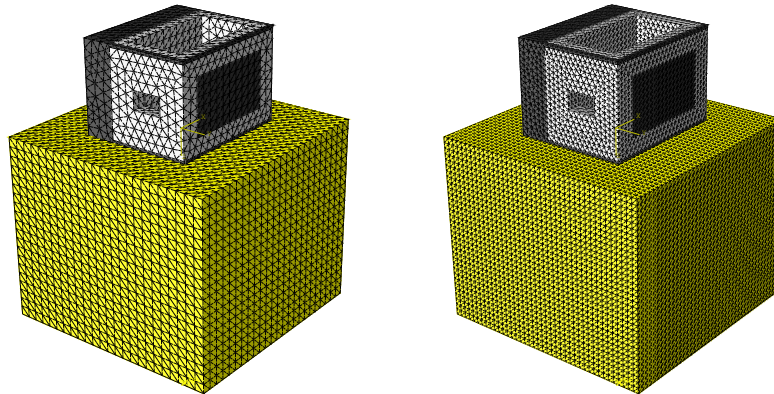


**Figure 6-5:** Examples of two mesh sizes employed during the convergence study of the model. On the left, the mesh size is 1 mm, while it measures 0.6 mm in the model on the right.

and displacements selected for the current study were within the linear elastic range observed in the experimental part of this work.

---

# Chapter 7

---

## Results

This chapter is divided into two main parts to differentiate between the results for the biomechanical testings and the computational study.

### 7-1 Biomechanical Study

#### 7-1-1 Stiffness of the implants

The compression tests for the evaluation of the cage stiffness,  $K_d$ , revealed the measurements given in Tab. 7-1 and 7-2 with  $p$ -values of 0.8046 and 0.3849 between the two porosities, respectively for the cervical and lumbar tests, thus indicating that the variations were not significant. Figure A 7-1 displays two bar-plots for the stiffness of the cervical implants on the left, and for the lumbar implants on the right.

Cervical Implants	
Stiffness (N/mm)	
P80	55277.52±11132.61
P70	49513.94±13414.42

**Table 7-1:** Stiffness for the cervical cages.

Lumbar Implants	
Stiffness (N/mm)	
P80	53036.97±11089.53
P70	47294.08±9667.70

**Table 7-2:** Stiffness for the lumbar cages.

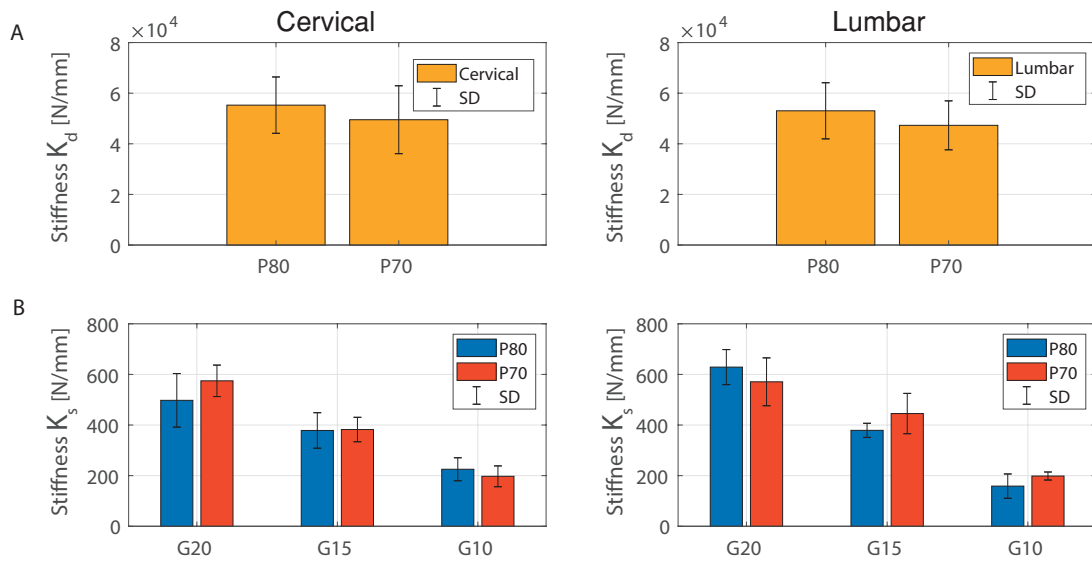


**Figure 7-1:** A) Graphic comparison of the mean stiffness values  $K_d$  of the cervical (left) and lumbar (right) implants, in the two porosities (P80, P70). B) Bar-plots displaying the mean stiffness values of the implant-foam systems,  $K_s$ , on the left for the cervical cages and on the right for the lumbar cages. The graphs present combinations with both porosities (P80, P70) and substrate densities (G20, G15, G10). In both A and B, the error bars indicate the standard deviations.

### 7-1-2 Stiffness and yield load of the system

The data extracted from the compression machine was used to compute the mechanical properties of the system composed of the implant-foam block. Tables 7-3 and 7-4 display the stiffness values,  $K_s$  and yield loads,  $F_y$ , of the cervical and lumbar set-ups respectively. The stiffness values resulted from linear regression between 50 and 150 N for all experiments, while the yield loads corresponded to the values found by plotting a line of slope  $K_s$  through the offset displacement. A feature for the experimental set-up was that the pushrod had to freely rotate on top of the spherical superior fixture. This caused for some experiments a toe region of approximately 0.7 mm for misalignment. Therefore, a slack correction rounded to 1 mm was applied, and consequently the displayed data ranges from 0 to 4 mm of displacement.

For both cervical and lumbar cages, the statistical analyses revealed no significant difference in the stiffness of the systems between the two porosities. On the other hand, the effect of substrate density was significant ( $p < 0.05$ ; order of  $10^{-13}$  for the lumbar cages and order of  $10^{-10}$  for the cervical implants). For the cervical implant, the statistical analysis revealed  $p = 0.475$  for the porosity parameter. From lower to higher substrate density, the stiffness values were respectively  $225.28 \pm 45.37$  N/mm,  $378.53 \pm 70.15$  N/mm and  $497.59 \pm 105.73$  N/mm for the most porous cage, versus  $197.39 \pm 41.13$  N/mm,  $382.27 \pm 48.26$  N/mm and  $574.64 \pm 62.16$  N/mm for the least porous cage. The change caused by substrate density was significant. Taking the medium-density foam as a reference, having the closest properties to healthy bone, the

system stiffness was twice the stiffness of the system with the lower density foam for P70, and 1.7 times for the higher porous cage. The stiffness of the system for the high-density foam was approximately 1.5 the value of the  $K_s$  for the medium-density foams for P70 ( $574.64 \pm 62.16$  N/mm versus  $382.27 \pm 48.26$  N/mm), and 1.3 times for P80 ( $497.59 \pm 105.73$  N/mm versus  $378.53 \pm 70.15$  N/mm).

In the systems with the lumbar cages,  $p = 0.619$  when comparing the cage porosities, indicating that the differences found were not significant. From lower to higher substrate density the  $K_s$  values were respectively  $158.65 \pm 47.99$  N/mm,  $379.03 \pm 27.87$  N/mm and  $628.87 \pm 69.25$  N/mm for P80, versus  $198.50 \pm 15.25$  N/mm,  $445.40 \pm 79.63$  N/mm and  $570.80 \pm 94.54$  N/mm for P70. As for the change in the substrate density,  $K_s$  for the medium-density foams was a little more than twice the one for the low-density foams. The bar-plots in Fig. B 7-1 display all the mean values of the extracted data for the cervical (left) and lumbar (right) implants. Figures 7-2 and 7-3 provide the force-displacement curve for all the tested cervical and lumbar combinations. The  $p$ -values for the overall interaction of the two parameters for the cervical and lumbar experiments were respectively 0.210 and 0.102. Figure A 7-4 shows the graphs comparing the mean curves with 95% confidence intervals for the different substrate densities, only for the cages of 20% apparent density. The image on the left refers to the data with the cervical cages, while the graph for the lumbar implants is on the right. These were obtained by averaging the data from the five repetitions, for each grade. The same curves for the P70 cages were not included since the first analysis revealed no statistical difference when changing the cage porosity. The curves were intersected with a line corresponding to the physiological loads, respectively of 250 N and 280 N for the cervical and lumbar experiments to find the corresponding mean deformation values. The triangle in the plots of Fig. A 7-4 indicate such intersection to highlight that such deformations stayed within the elastic region of the systems, with the exception of the low-density substrate for the cervical system.

---

 Cervical
 

---

	Low-Density Substrate		Medium-Density Substrate		High-Density Substrate	
	Stiffness (N/mm)	Yield Load (N)	Stiffness (N/mm)	Yield Load (N)	Stiffness (N/mm)	Yield Load (N)
P80	$225.28 \pm 45.37$	$375.09 \pm 27.86$	$378.53 \pm 70.15$	$811.60 \pm 56.98$	$497.59 \pm 105.73$	$1033.38 \pm 95.66$
P70	$197.39 \pm 41.13$	$385.85 \pm 57.07$	$382.27 \pm 48.26$	$784.51 \pm 59.71$	$574.64 \pm 62.16$	$941.53 \pm 39.01$

**Table 7-3:** Stiffness and yield load of the systems with the cervical cages.

---

 Lumbar
 

---

	Low-Density Substrate		Medium-Density Substrate		High-Density Substrate	
	Stiffness (N/mm)	Yield Load (N)	Stiffness (N/mm)	Yield Load (N)	Stiffness (N/mm)	Yield Load (N)
P80	$158.65 \pm 47.99$	$390.54 \pm 29.21$	$379.03 \pm 27.87$	$825.49 \pm 43.79$	$628.87 \pm 69.25$	$1062.87 \pm 43.06$
P70	$198.50 \pm 15.25$	$399.84 \pm 48.46$	$445.40 \pm 79.63$	$817.53 \pm 45.06$	$570.80 \pm 94.54$	$1046.76 \pm 35.25$

**Table 7-4:** Stiffness and yield load of the systems with the lumbar cages.

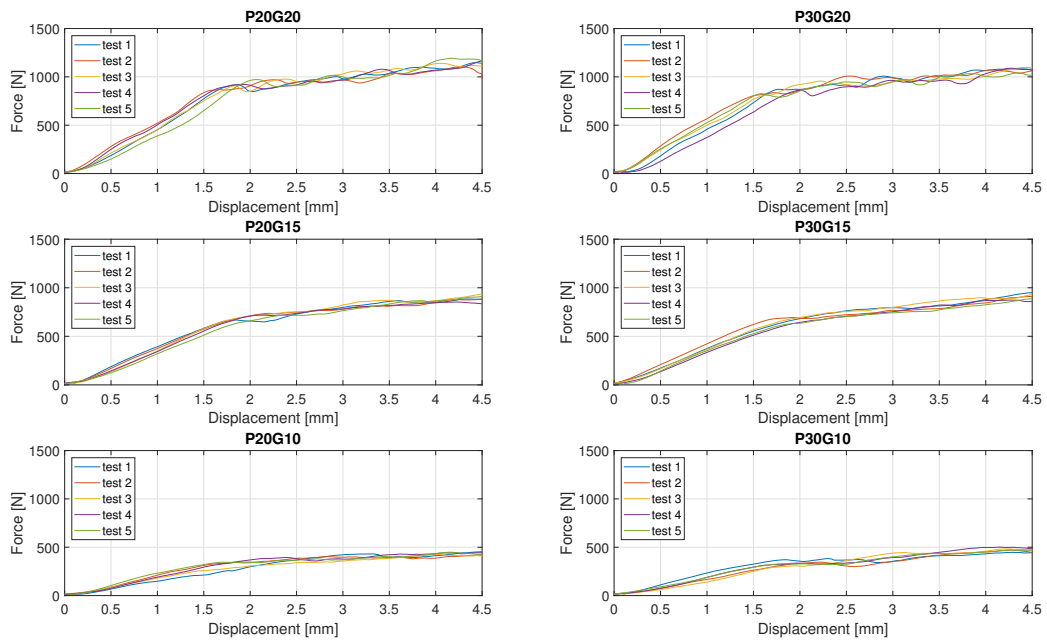


**Figure 7-2:** Force-displacement curves for the cervical implant-foam systems.

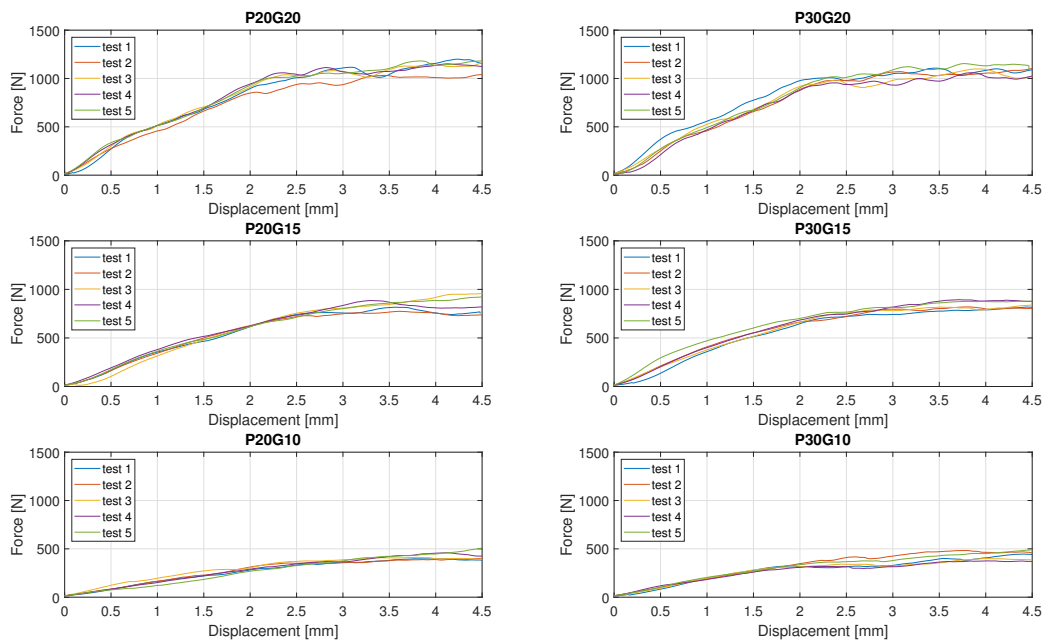


**Figure 7-3:** Force-displacement curves for the lumbar implant-foam systems.

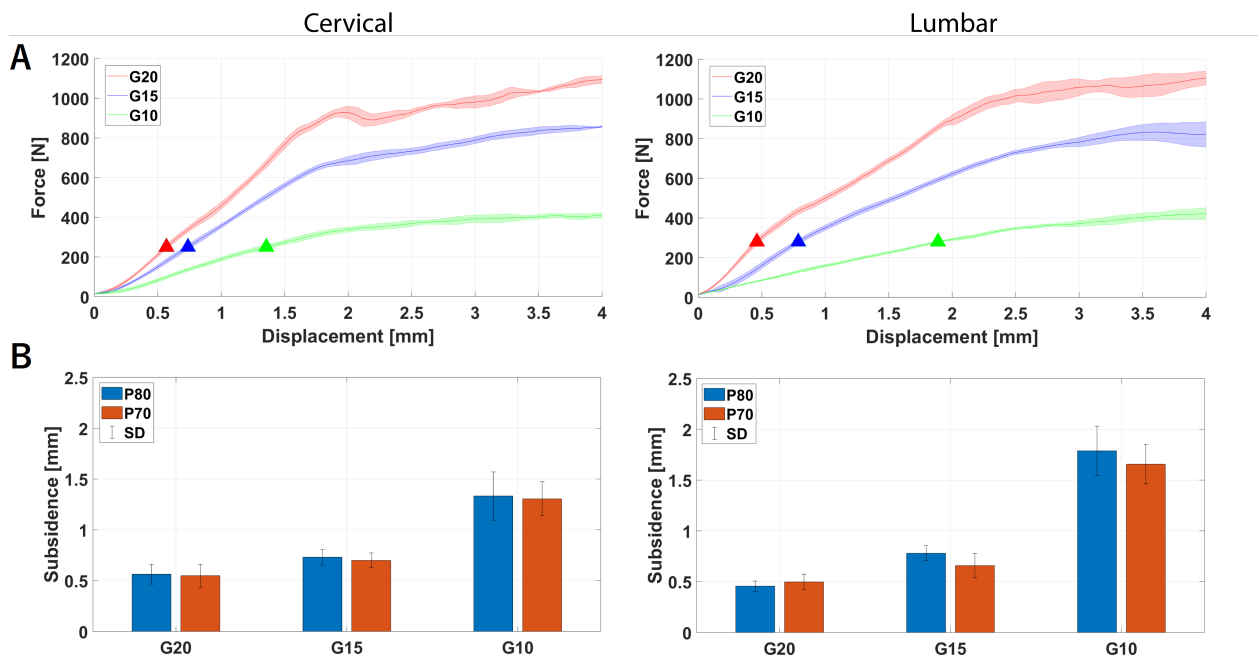


**Figure 7-4:** A) Force-displacement curves for the cervical cages on the left, and the lumbar cages on the right. Each graph displays three curves of the means and 95% confidence interval of the tests performed with the three foam densities (G20, G15, G10). The data represented is for the cage with 20% apparent density (P80). B) Bar-plots displaying subsidence at physiological loading (250 N for cervical and 280 N for lumbar implants) for all the foam grades and porosity combinations. The left graph refers to the experiments for the cervical implants, while the one of the right is for the lumbar implants. The error bars indicate the standard deviations.

### 7-1-3 Stiffness of the polyurethane foam blocks

Cervical			
Stiffness of the polyurethane foams $K_p$ (N/mm)			
	Low-Density Foam Substrate	Medium-Density Foam Substrate	High-Density Foam Substrate
P80	226.20±79.01	381.15±129.83	502.11±178.95
P70	198.18±86.57	385.24±155.95	581.38±232.72

**Table 7-5:** Stiffness of the polyurethane foams extracted from the systems with cervical cages.

Lumbar			
Stiffness of the polyurethane foams $K_p$ (N/mm)			
	Low-Density Foam Substrate	Medium-Density Foam Substrate	High-Density Foam Substrate
P80	159.12±67.36	381.76±116.72	636.41±201.87
P70	199.34±32.11	449.63±102.18	577.78±125.47

**Table 7-6:** Stiffness of the polyurethane foams extracted from the systems with lumbar cages.

The stiffness of the polyurethane foam blocks,  $K_p$ , for each set of experiments was evaluated by modeling the subsidence testing system as two springs in series as suggested in the standard. The resulting equation was:

$$K_p = \frac{K_s K_d}{K_d - K_s} \quad (7-1)$$

where  $K_s$  was the stiffness of the system obtained from the compression machine, while  $K_d$  represented the device stiffness from the compression tests with the metal blocks. The standard deviations were evaluated through error propagation equations. Indicating the denominator of Eq. 7-1 as an arbitrary variable  $K_c$ , the uncertainty between the subtracting terms,  $\delta K_c$ , was evaluated as follows:

$$K_c = K_d - K_s \quad (7-2)$$

$$\delta K_c = \sqrt{\delta K_d^2 + \delta K_s^2} \quad (7-3)$$

The resulting uncertainty  $\delta K_c$  was plugged into Eq. 7-4 to compute the uncertainty  $\delta K_p$ .

$$\delta K_p = K_p \sqrt{\left(\frac{\delta K_d}{K_d}\right)^2 + \left(\frac{\delta K_s}{K_s}\right)^2 + \left(\frac{\delta K_c}{K_c}\right)^2} \quad (7-4)$$

The uncertainty resulting from Eq. 7-4 referred to the standard deviation for the foam stiffness  $K_p$ . The results are summarized in Tables 7-5 and 7-6. The statistical analysis

revealed that there was a significant difference with the variations in foam density ( $p = 0.0239$  for the lumbar tests and  $p = 0.0269$  for the cervical ones) while there was no significant difference by changing between P80 and P70 ( $p = 0.725$  for the lumbar and  $p = 0.629$  for the cervical).

#### 7-1-4 Subsidence

Subsidence was higher in the low-density foam, as a consequence of the lower compressive modulus of the foam. The differences among the three foam grades were significant in both the cervical and lumbar cases, whereas the change of cage porosity had no effect. Subsidence was compared and displayed in bar graphs in Fig. 7-4. Similarly to what was observed for the comparison of the stiffness of the systems, the change of the apparent density of the cages had no significant effect on subsidence ( $p = 0.602$  for the cervical cages;  $p = 0.202$  for the lumbar cages). Contrarily, the change of substrate density provoked statistically significant changes in the measured subsidence. For the cervical cages, subsidence in the medium-density foams was approximately 20% more than the ones measured for both apparent density values in the high-density foams. When comparing the medium-density with the low-density foams, subsidence was found to increase by 45% in the lower density material. For the lumbar cages the low-density foam saw almost a 60% increase in subsidence compared to the medium-density substrate for both apparent density values. Instead, the denser substrate reduced subsidence by 24% for P70 and 41% for P80.

Subsidence of the cervical implants at 250 N (mm)			
	High-Density Substrate	Medium-Density Substrate	Low-Density Substrate
P80	0.564±0.099	0.731±0.077	1.333±0.237
P70	0.549±0.112	0.699±0.071	1.305±0.166

**Table 7-7:** Subsidence at 250 N for the cervical implants with different porosities (P80, P70) combined with substrates of three densities.

Subsidence of the lumbar implants at 280 N (mm)			
	High-Density Substrate	Medium-Density Substrate	Low-Density Substrate
P80	0.456±0.051	0.779±0.072	1.787±0.243
P70	0.497±0.075	0.658±0.121	1.657±0.194

**Table 7-8:** Subsidence at 280 N for the lumbar implants with different porosities (P80, P70) combined with substrates of three densities.

#### 7-1-5 Digital Image Correlation Data

Since the image recording was triggered manually, the first step for the post-processing of the images from the DIC setup was to remove the data prior to reaching the preload value of 15 N. This allowed to have the image corresponding to the preload value as

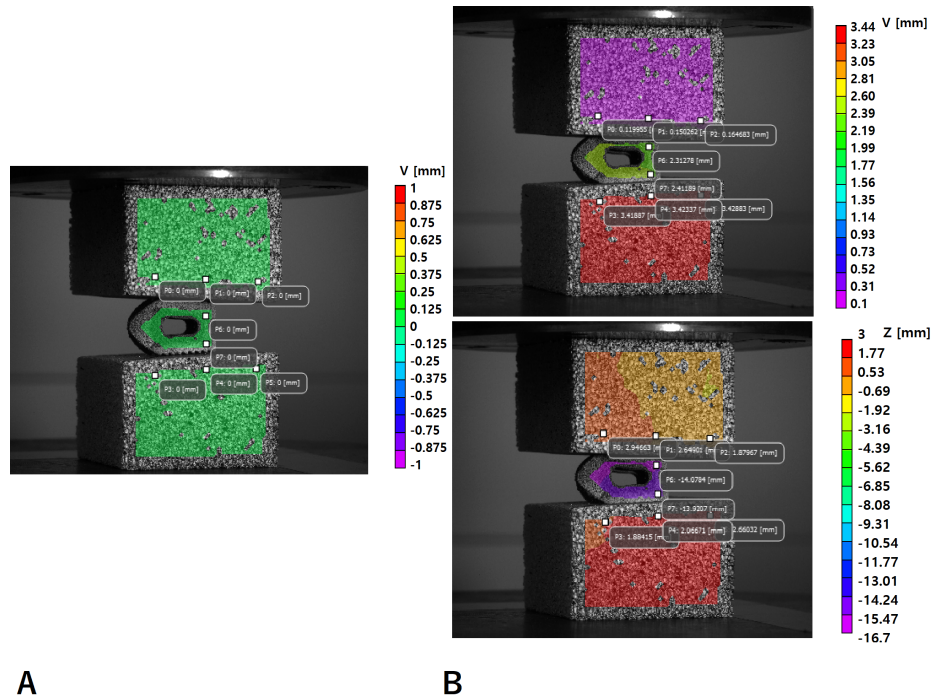


**Figure 7-5:** Figure A shows the reference image, in which the displacement distribution along the load direction is zero throughout the system. Figure B shows a capture at 780N arbitrarily chosen to illustrate an example of the measured displacement distribution along the  $y$  and  $z$  axes (refer to Fig. 7-6 for the coordinate system). Three points on the top and bottom foams respectively are selected, as well as two points on the cage.

the reference image for the following displacement calculations. Figure 7-5 illustrates the reference image for the displacement calculations with the selected points for observation. Three points were selected, i.e. at the top and bottom foams, from left to right, to check any rotation occurring around the  $z$ -axis, with reference to the coordinate system in Fig. 7-6. The occurrence of foam rotation was verified by comparing the values of the deformations along the  $y$ -axis, indicated as  $V$  in the post-processor, of adjacent reference points. No rotation of the foams was registered, as there was an average variation of less than 0.01 mm.

Furthermore, two points were selected, i.e. the top and bottom of the cage to extract displacements in the  $z$ -axis due to the tilting around the  $x$ -axis, parallel to the page. These reference points were used to verify that the tilting was not occurring before the physiological load was reached, by comparing the deformation along  $z$  referred to as  $W$ . The difference in deformation of 1 mm between the top and bottom references on the cage translated into the tilting, and was easily spotted by viewing the images. The tilting occurred at different mean loads according to the grade, but always way above the physiological load. For the high-density foam tilting occurred at approximately  $970 \pm 68$  N, for the medium-density foam at  $770 \pm 74$  N, and for the low-density at  $480 \pm 68$  N.

The main purpose of using the DIC system was to verify that subsidence was occurring

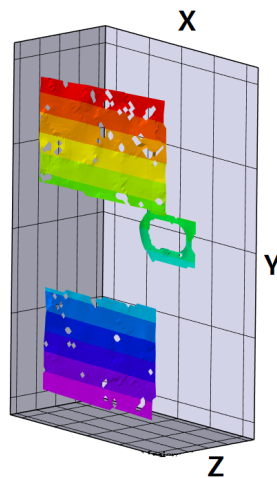


**Figure 7-6:** 3D plot of the set-up showing the reference axes in the Vic3D post-processing software.

Lumbar		
$E_0 - E_1$ [%] at 280 N		
	Medium-Density Foam Substrate	High-Density Foam Substrate
P80	$0.22 \pm 0.1$	$0.48 \pm 0.1$
P70	$0.16 \pm 0.2$	$0.15 \pm 0.1$

**Table 7-9:** Average and SD of  $E_0 - E_1$  at physiological loading, 280 N in percentage, over all the repetitions for the experiments post-processed with DIC.  $E_0$  (Eq. 5-2) referred to the change of length between the top foam and the implant, while  $E_1$  indicated the change of length between the bottom block and the implant.

symmetrically, through the method explained in the previous chapter. Figure 7-7 displays an example of the applied post-processing tool, while Tab. 7-9 shows the average differences between the extensometers applied respectively between the top and bottom foams and the implant. With reference to the formula in Eq. 5-2,  $E_0$  was used to indicate the change of length between the superior block and the implant, while  $E_1$  was for the lower block. For each of the five repetitions combining the high- and medium-density foam with the P80 and P70 cages,  $E_0$  and  $E_1$  were extracted and averaged. The differences of the averages were reported in percentages and the results demonstrated that subsidence was occurring symmetrically within the range of loads of interest.

The strains were also computed with the software and it was verified that strain changes were in the order of magnitude of  $10^{-6}$  mm in all directions, therefore did not interfere with the measured subsidence. The use of the extensometer tool was possible for the lumbar cage combinations with the medium- and high-density foams, but was not possible for the low-density foam and for none of the experiments with the cervical cage, due to the inability to create the plot of the speckle pattern by the software. Although DIC is known for being an unsuitable method for accurate measurements of

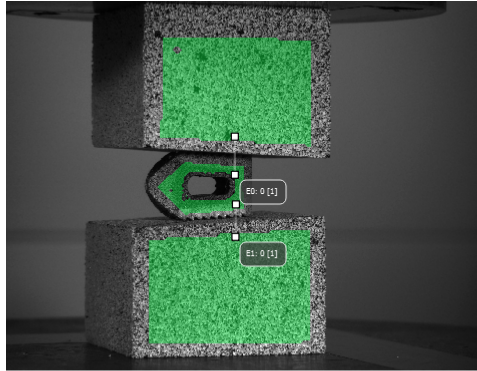


**Figure 7-7:** Application of extensometers to check differences in the change of length between the top foam-implant, and bottom foam-implant. The extensometers were aligned along the centre of the foams-cages for all experiments.

porous materials, it helped monitoring the changes at macro-scale, such as the tilting and symmetrical behaviours, and could be considered for similar purposes in analogous studies.

## 7-2 Computational Study

### 7-2-1 Stiffness of the implants

Stiffness of the cage (N/mm)					
	FP	C0	C20	C40	FS
P70	15679.22	17131.03	21512.69	25233.15	516924.1
P80	7508.86	10489.91	13462.47	16370.15	
P90	1968.229	5631.296	7553.612	9775.076	

**Table 7-10:** Stiffness of the cage with all combinations of porosities (P70, P80, P90) and solid-to-porous ratios (FP, C0, C20, C40, FS).

The stiffness values for all the combinations of porosities and solid-to-porous ratios are reported in Tab. 7-10, ranging from the lowest porosity, P70, to the highest P90, and from the fully porous to the fully solid titanium cages. The bar-plot in Fig. A 7-8 helps with the comparison of all the resulting stiffness values, with the exception of the stiffness for the fully solid cage being greater than all the other values of one order of magnitude. The comparison revealed that the stiffness was influenced by porosity changes for the simplified cage design. Moreover, the stiffness increased with the increase of solid-to-porous ratio, from fully porous to the fully solid cage. The stiffness decrease from P70 to P90 was 87% for the FP implant, 67% for C0, 64% for C20, and 61% for C40, demonstrating that the increase of the solid-to-porous ratio decreased the effect of the change in porosity. Furthermore the stiffness decrease from

C40 to C20 was around 22% for P90, 17% for P80, and 14% for P70.

### 7-2-2 Stiffness of the implant-foam system

Stiffness of the system using C0 (N/mm)			
	Low-Density Substrate	Medium-Density Substrate	High-Density Substrate
P70	413.803	1211.32	2371.88
P80	410.5511	1185.306	2278.405
P90	395.1515	1074.24	1921.76

**Table 7-11:** Stiffness of the implant-substrate system using the cage with 0% solid titanium frame (C0) for all the foam densities and porosities (P70, P80, P90) combinations.

Stiffness of the system using C20 (N/mm)			
	Low-Density Substrate	Medium-Density Substrate	High-Density Substrate
P70	414.29	1215.55	2388.20
P80	411.58	1193.82	2309.64
P90	399.12	1102.23	2008.23

**Table 7-12:** Stiffness of the implant-substrate system using the cage with 20% solid titanium frame (C20) for all the foam densities and porosities (P70, P80, P90) combinations.

Stiffness of the system using C40 (N/mm)			
	Low-Density Substrate	Medium-Density Substrate	High-Density Substrate
P70	414.63	1218.37	2398.69
P80	412.34	1199.69	2330.52
P90	402.29	1123.24	2072.29

**Table 7-13:** Stiffness of the implant-substrate system using the cage with 40% solid titanium frame (C40) for all the foam densities and porosities (P70, P80, P90) combinations.

The stiffness values ranged from 413.803 N/mm, which was the minimum value corresponding to the most porous implant with the low-density substrate in the C0 cage, to 2398.698 N/mm for the C40 cage combined with the lowest porosity and greatest foam density. An overview of all the stiffness values for the implant-foam system is shown in Tab. 7-11, 7-12 and 7-13, while a graphic representation is provided in Fig. A 7-9. The stiffness values of the assemblies of same porosity cages and foam grade over the different solid-to-porous ratios underwent slight variations, in the order of  $10^1$ . The same applied to the effect of the porosity change, when comparing systems with constant foam grade and solid-to-porous ratios. In accordance with the results of the biomechanical study, the variation in cage porosity did not provoke changes in the overall stiffness, while the change of substrate density was significant. Figure B 7-9 exhibits

an example of displacement distribution when comparing systems with same porosity and foam grade over different frame thickness.

### 7-2-3 Subsidence

Tables 7-14, 7-15 and 7-16 present an overview of the computed subsidence as the maximum displacement value observed at the implant-block interface. Figure 7-10 displays the comparison of the displacement distribution on the surface of the block interfacing the implant over different foam grades. The stress distribution did not undergo changes when using the same frame thickness over different porosities.

Subsidence for C0 (mm)			
	Low-Density Substrate	Medium-Density Substrate	High-Density Substrate
P70	0.694	0.236	0.121
P80	0.698	0.243	0.131
P90	0.736	0.225	0.115

**Table 7-14:** Subsidence as maximum displacement of the top surface of the block using the cage with 0% solid titanium frame (C0) for all the foam densities and porosities (P70, P80, P90) combinations.

Subsidence for C20 (mm)			
	Low-Density Substrate	Medium-Density Substrate	High-Density Substrate
P70	0.694	0.236	0.120
P80	0.699	0.240	0.128
P90	0.723	0.213	0.120

**Table 7-15:** Subsidence as maximum displacement of the top surface of the block using the cage with 20% solid titanium frame (C20) for all the foam densities and porosities (P70, P80, P90) combinations.

Subsidence for C40 (mm)			
	Low-Density Substrate	Medium-Density Substrate	High-Density Substrate
P70	0.693	0.236	0.114
P80	0.698	0.239	0.115
P90	0.714	0.229	0.126

**Table 7-16:** Subsidence as maximum displacement of the top surface of the block using the cage with 40% solid titanium frame (C40) for all the foam densities and porosities (P70, P80, P90) combinations.

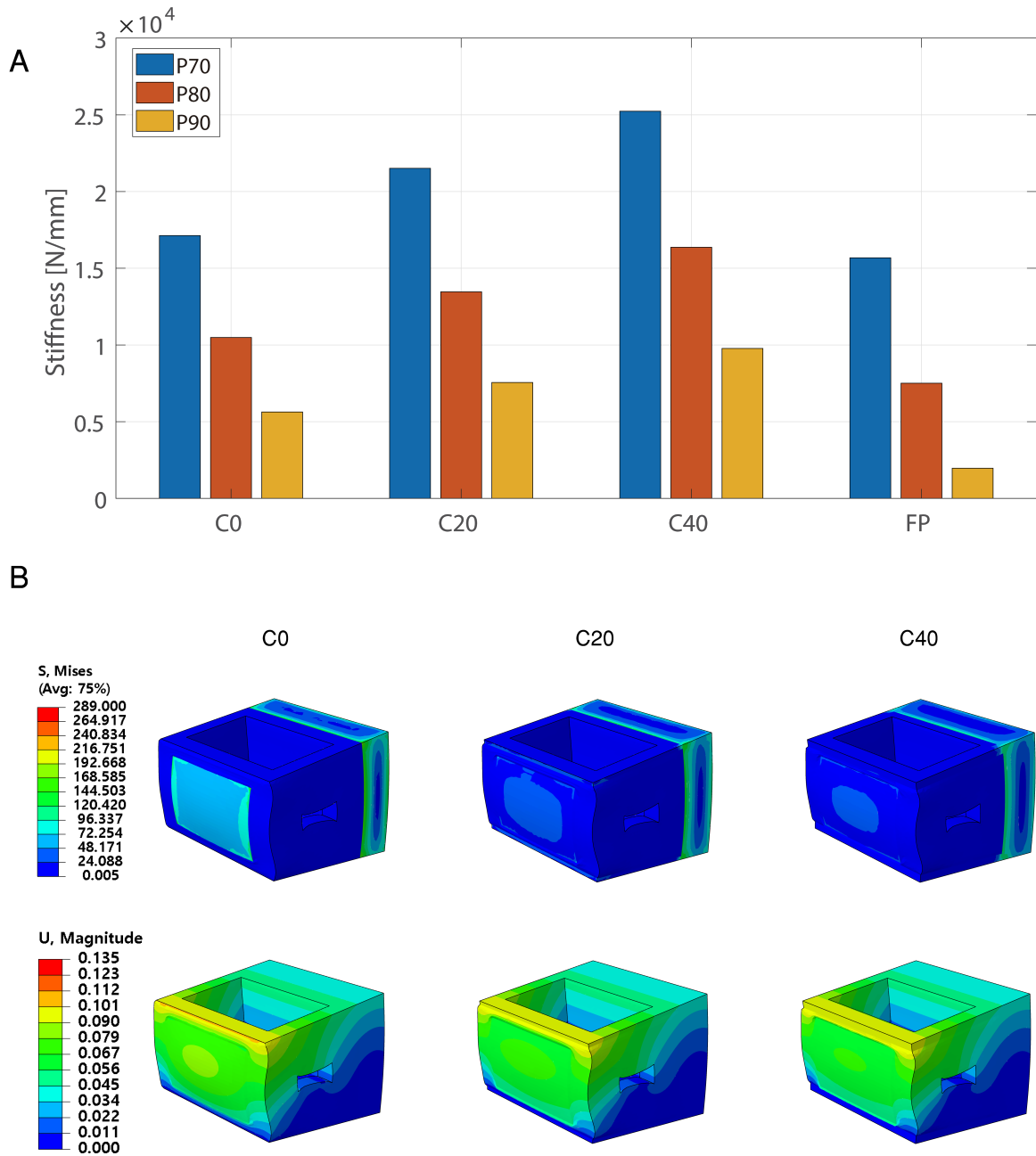


**Figure 7-8:** A) Bar-plots displaying the stiffness of the cages for the all porosities (P70, P80, P90) and frame thickness (C0, C20, C40) combinations. B) From the top, stress and displacement distributions comparison with constant porosity P90 and variable frame thickness. From left to right, C0, C20 and C40.

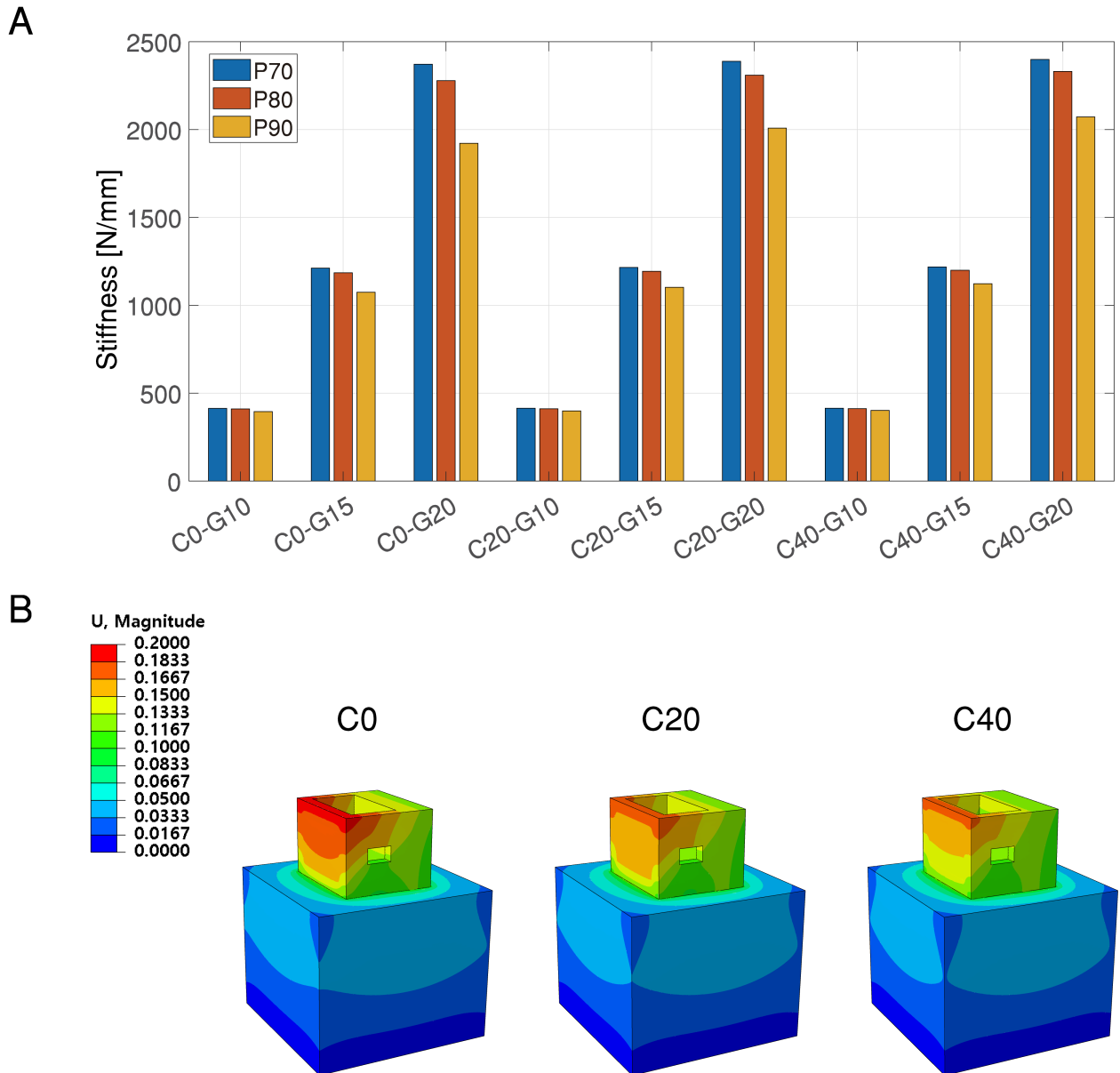


**Figure 7-9:** A) Bar plot displaying the implant-substrate system stiffness using the models with 0% (C0), 20% (C20) and 40% (C40) solid frame with all combinations of porosities and foam grades. B) Example of the comparison of displacement distribution for the cages C0, C20 and C40, with constant porosity P90 and foam density G20.

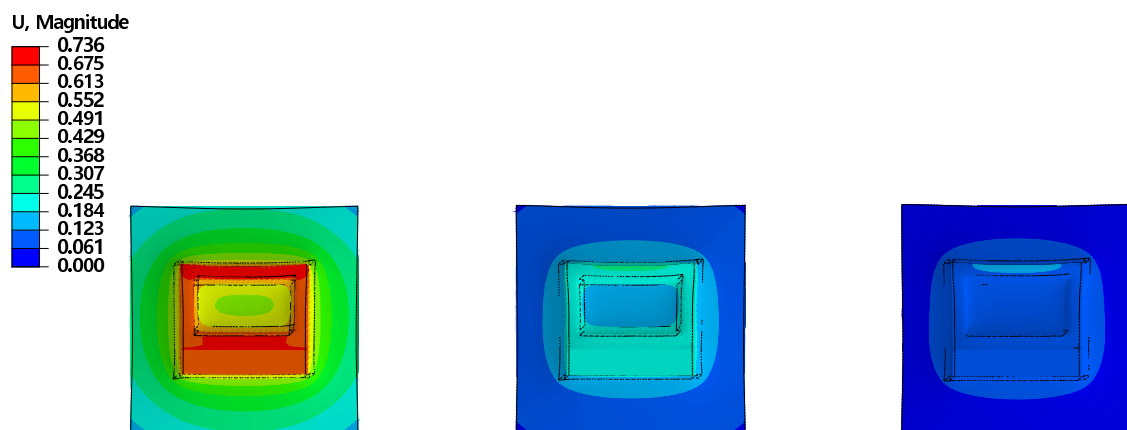


**Figure 7-10:** Displacement distribution of the block surface interfacing with the implant. From left to right, the foam densities were G10, G15 and G20 for the simulations with constant porosity P90 and cage C0.



---

# Chapter 8

---

## Discussion

This section presents extensive discussion on the findings, related to the outcomes of previous studies in the literature and to the research questions outlined in Chapter 4.

### 8-1 Spinal cage porosity and bone density

#### 8-1-1 Mechanical properties of porous spinal cages

The experiments of this thesis did not reveal any significant effect of the change of apparent density of the cage on subsidence. The hypothesis was that lower stiffness of the overall system would be observed by using a cage with greater porosity, indicating lower stresses at the implant-bone interface, and consequently a lower risk of subsidence. The implants used in this study featured a titanium frame surrounding a lattice of diamond unit cells. Two types of cages were tested which differed from each other in apparent density by 10%. Specifically, the lighter cage (P80) was characterized by a lattice with Young's modulus of 1577.5 MPa, while the heavier one (P70) had elastic modulus of 3328.4 MPa, with reference to the work of Ahmadi et al. [14] and as validated by a finite element model. Although the lattices in the two cages differed in Young's modulus by approximately 71%, the stiffness of the systems with the cervical implants during the compression tests to measure subsidence varied only by 13% for the low-density foam, 1% for the medium-density foam and 14% for the high-density foam. For the lumbar cages the differences in percentage of the system stiffness from the lower to the higher-density foams were respectively 14%, 16% and 9.5%. The variations in both the lumbar and cervical cases could not be considered statistically relevant. The same was found for the stiffness measurements of the lumbar cages, where the P70 cage increased in stiffness by only 4% compared to the P80 cage. In a computational study conducted by Zhang et al.[98], the range of motion (ROM) of the spine, cage and endplate stresses were compared between an intact spine and different

surgical models with various cages. Among the analyzed implants, three types of fully porous and partially porous devices with 65%, 75% and 80% porosity were modelled through the determination of their mechanical properties. The data was retrieved from a previous mechanical study [114] which made use of a lattice with an eight-pillar unit cell. Interestingly, Zhang et al. reported a difference of almost 79% between the Young's moduli of the 75% and the 80% porosity samples, which caused greater distinction in the simulated endplate stress than the cage stress. Moreover, the variation between porosity was significant only for the maximum stresses of the endplates evaluated for the fully porous implants. These findings helped in triggering some considerations for the current study. A 5% change of porosity, from 80% to 75%, reported by Zhang et al. had a greater effect on the variation of Young's modulus ( $\approx 79\%$ ) compared to the 10% change using the diamond unit cell which was found to provoke a 71% variation. In a partially porous implant, such as the ones used for this study, when changing the porosity there were no major effects on the maximum stresses of the cage and the endplates, unlike what was found for the fully porous implants. Since the partially porous devices are thought to have the outer frame in the solid material with a porous inner part, the findings of the current biomechanical study supported the question for the research: *could the lack of stiffness variation in the implant and in the overall system be an effect of the presence of the frame in solid titanium?* In fact, the outer frame in the designed cages had apparently narrower area than the regions designated for the lattice, but in terms of contact area, the smooth titanium had greater contact area. This means that the effects given by the changes in the inner porous core could be hypothesized to be attenuated by the unvaried outer frame. This consideration led to the development of the finite element model to explore the influence of the frame thickness, of which outcomes are discussed in the next section. From a mechanical perspective, the idea of having a range of implants differing in apparent density for the purpose of achieving an optimal bone-implant interface revealed to be ineffective.

### 8-1-2 Implications of the findings for the *in-vivo* performance

If considering the *in-vivo* performance of the implant, the lack of variation of the mechanical properties when changing porosity can be advantageous. Van Bael et al. [115] for instance studied the seeding of human periosteum-derived cells combining three different pore shapes in two sizes for selective laser-melted Ti6Al4V scaffolds. Even though only two dimensions were analyzed, the study interestingly concluded that incorporating smaller and bigger pores in a lattice, and of locating them functionally within the structure would lead to improving both the seeding and proliferation of cells. In fact, wider pores of 1000  $\mu\text{m}$  are beneficial for nutrients and fluid flow, but when the cells are in their initial seeding phase, lower permeability, obtained by narrower pores (500  $\mu\text{m}$ ), is helpful for their attachment. Therefore, ideally the wider pores should be in the inner parts of the lattice, while the narrow pores would improve the initial seeding in the peripheral cage. As a lower limit of the diameter, it was observed that pores should be at least 100  $\mu\text{m}$  to allow good bone ingrowth [116]. Tissue growth was also found to be more responsive to local curvature [117], therefore this should be taken into consideration when designing the structure layout. Furthermore, different treatments to

control wettability of titanium have been investigated [118][119][120], which represents an interesting property for orthopaedic implants. Depending on the contact angle formed between surface and liquid, a material can be hydrophilic or hydrophobic, Fig. 8-1. In the first case, the angle is greater than  $90^\circ$ , while in the latter it is acute, resulting in a smaller contact area. Gittens et al. [121] reviewed different studies on contact angles of dental implant surfaces and highlighted an analogous consideration outlined earlier for permeability. A hydrophilic behavior can be beneficial in the cell adhesion stage, but research has shown this could also provoke reduced cell motility, thus loss in cell functions once they are seeded. All these aspects need to be investigated in combination in order to find an optimal condition.

Although porosity is important to trigger cell proliferation, its assessment needs

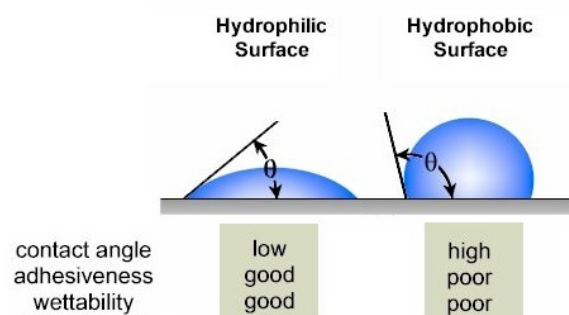


**Figure 8-1:** Contact angle in hydrophilic and hydrophobic surfaces. Image retrieved from [15].

to go beyond the purposes of tissue engineering. For instance, it has to have good manufacturability, while withstanding the compressive forces in the spine. Therefore the lack of differences in the mechanical performance between the P80 and P70 implants in the present research could be considered advantageous, opening the opportunity to further study the biological effects of employing different lattices, with the certainty of being mechanically adequate. Furthermore, with the findings of the current study suggesting that there is no difference in mechanical properties caused by varying the porosity, the manufacturing of implants featuring functionally graded lattices could be considered, from which fusion would greatly benefit.

### 8-1-3 Polyurethane foams for biomechanical tests of different bone densities

The current work also highlighted that the change of bone mineral density at the interface with the implant has a significant effect on subsidence occurrence, which is in accordance with previous studies [17][122][36] [77]. The degree of influence was assessed with the employment of three foam densities, to simulate low, average and above-average bone conditions. For all the mechanical testings and the simulations, the change in foam density was significant. While three variants of the bone condition were evaluated, the most interesting findings to comment upon are the differences between the medium- and low- density foams. The reason for this is that the medium-density foam was used to simulate the average condition of bone, while the low-density foam can be easily related to the condition of bone in osteoporotic patients, while the

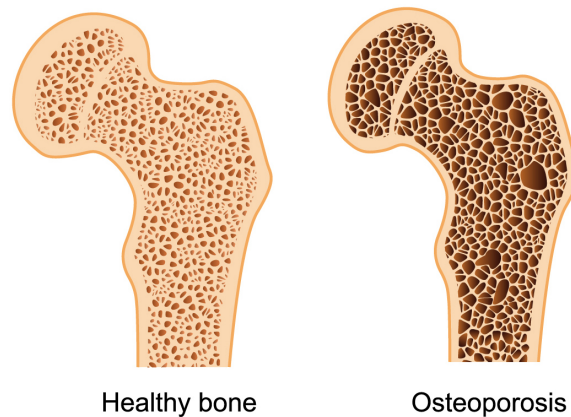


**Figure 8-2:** Comparison between healthy and osteoporotic bone. Image retrieved from [16].

high-density foam was used to provide a wider range to prove the influence of BMD. Figure 8-2 provides a visual representation of the lesser dense osteoporotic bone. Starting from the analysis on the stiffness of the implant-foam systems, for the P70 cervical implant the system stiffness decreased by 40.5% and 48% for P80, while the change in stiffness for the lumbar implants was about 10% higher than the values observed for the corresponding systems with cervical implants. The plots of the force-displacement curves in A 7-4 highlight the effect deriving from the change in substrate density, revealing also a slightly greater difference when comparing the systems with the medium- and low-density foams instead of the comparison between the medium- and high-density foams. The same decrease percentages were observed in the calculated stiffness for the foams. It should be noted that the evaluation on the error propagation was conducted, which resulted in high uncertainty values at approximately the same order of magnitude of the corresponding mean values. Furthermore, subsidence decreased around 20% between the medium- and low-density for both cages. Suh et al. [17] demonstrated in their study that the most influential factor for implant performance is the condition of the underlying bone, when comparing it with factors such as cage size and material. The group investigated different cages complying to the ASTM-F2267 standard for load induced subsidence, and in order to evaluate the influence of the underlying bone, they tested using two foam grades. According to the nomenclature in ASTM-F1839, the selected foams were grade 20, with a density of  $320.4 \text{ kg/m}^3$ , and was intended to mimic the case where the cartilaginous endplate is preserved, and grade 10 of  $160.2 \text{ kg/m}^3$  to model the case in which the endplate is totally removed and the implant is directly in contact with trabecular bone. Although being useful to highlight the influence of bone density, the experiment conducted by the group should not be considered representative of their desired scenarios. ASTM-F2267 indicated grade 15 for subsidence testing because it represents the average properties of trabecular bone, but to investigate the influence of bone density it made sense to test using a different foam grade. What could be questionable in the study conducted by Suh et al. was found to be the rationale behind the use of the two grades. Rigid polyurethane foams are widely used for biomechanical testing and their composition is standardized in ASTM-F1839. In X1.2 of the appendix, it is stated that these foams



**Figure 8-3:** Cervical cages in  $\text{Si}_3\text{N}_4$  used for the study by Suh et al. [17]. On the left, the cage with an empty core; on the right, the cage core is filled with load-bearing porous  $\text{Si}_3\text{N}_4$ .

exhibit mechanical properties which are similar to cancellous bone. Comparing for instance only the Young's modulus for both cancellous and cortical bone, they are respectively 100 MPa and 12000 MPa [123]. This means that the polyurethane foam could never be used to mimic a case in which cortical bone is preserved, as it was intended by Suh et al. The materials used in their study come from Sawbones, whose website provides a catalog of the different grades and corresponding mechanical properties. Grade 20 has 137.0 MPa for compressive modulus, which is far from reaching the value for cortical bone. It would be correct to consider the two models as variations of quality of bone according to bone mineral density, as it was done in the current study. The findings of the current work confirm the need for the preliminary assessment of the bone density for predicting the risk of subsidence and to investigate possible solutions. Moreover, two main reasons lead this work to focus on the interaction of implants with poor bone quality. The first was found in one of the results from the study of Suh et al. [17]. When they compared subsidence over two foam densities with two  $\text{Si}_3\text{N}_4$  cages, one with an empty core and the other with the core filled with load-bearing porous  $\text{Si}_3\text{N}_4$  8-3, it was found that subsidence significantly reduced in the cages with the porous core, but only in the tests which used the lower density foam. This indicated that implant preparation and selection could be crucial in patients with poorer bone quality, whereas in the case of denser bone the influence of porous cores, morphology and material are all less significant. The other reason relied on data available about the characteristics of patients in the United States undergoing spinal fusion between 1998 and 2008. The mean age for cervical fusion patients was 53.3, for thoracic fusion 42.7 and lumbar fusion 56.3. Furthermore, in the indicated time span, there was an increase of 239.2% of annual number of discharges for patients aged 65 and older, which could not be explained with the increase of the aging population alone [124]. This data is concerning and indicates the need to push for better solutions with attention to bone mineral density since it was demonstrated that bone mineral density decreases with aging, especially for young adulthood in women [18], with a greater decrease in the cases of osteoporotic patients. The comparison of BMD values for the lumbar spine is shown in Fig. 8-4 and revealed a mean of  $0.963 \text{ g/cm}^3$  for healthy females against  $0.777 \text{ g/cm}^3$  for females with osteoporosis. In healthy men, the diminution of BMD with aging was minimal and became significant after age 85, according to the same study. In Fig. 8-5 a comparison between men and female reduction is highlighted.

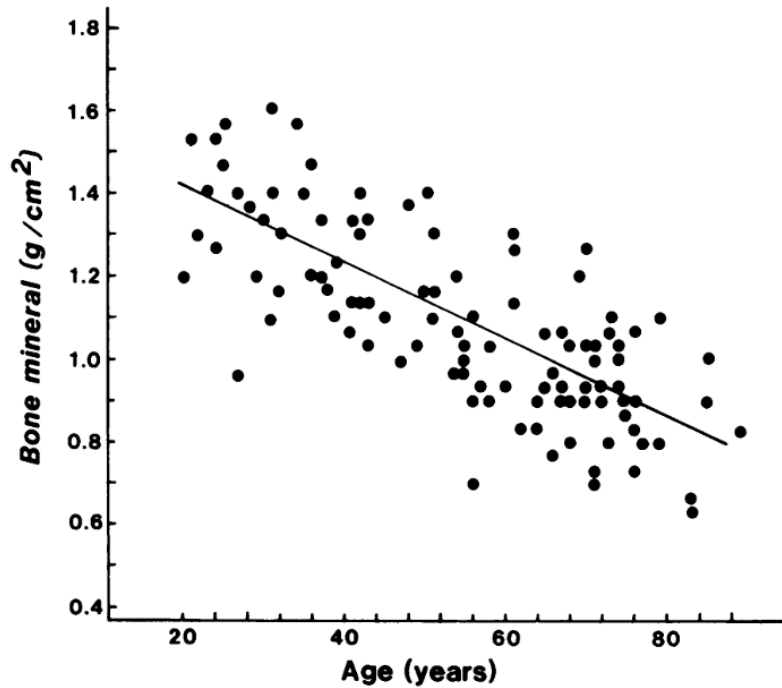


**Figure 8-4:** BMD of lumbar spine in a group of 105 women. Data is part of the work of Rigg's et al.[18]

As a consequence of all that was discussed, more studies should be done in order to improve the current products for spinal fusion with the greatest attention to the interaction with bone. Moreover, better surgical planning could be proposed based on predictions following an evaluation for bone mineral density. An example is provided by Schreiber's work [125], in which correlation was obtained between Hounsfield unit (HU) and BMD, enabling identification of patients with diminished bone density. Polyurethane foam was used to execute biomechanical experiments, validating the correlation between HU and compressive strength. This would help in predicting the outcome of a surgery and if no suitable solutions are available for a poor bone quality, the avoidance of the surgery could be considered, which would reduce the risk of revision surgery and be more cost effective.

## 8-2 Thickness of the cage frame in solid titanium

While for the biomechanical study the lack of change in stiffness was assumed to be caused by the presence of the constant outer frame with a high Young's modulus, the computational study was used to explore the influence of the thickness of the outer frame on the stiffness of the implant and the implant-bone system. The three models of the simplified cervical cages featured a frame of 1.5 mm, featuring 0% solid titanium in the cage C0, 20% in C20 and 40% in C40. The percentages were chosen arbitrarily taking into consideration the real implant design and realistic ratios in terms of manu-

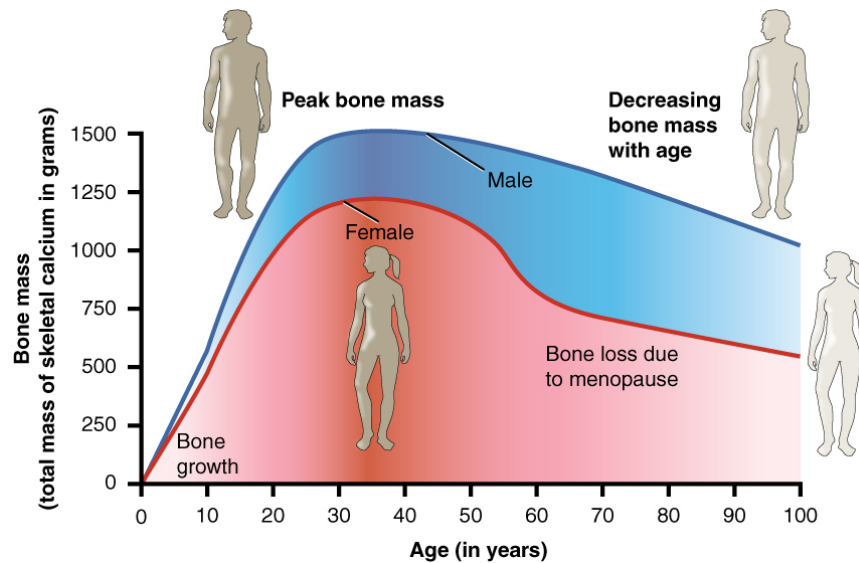


**Figure 8-5:** Trends of bone mass for female and with aging. Image retrieved from *Anatomy & Physiology* by Young et al. [19]

facturability and strength of the cage. The results revealed almost no differences when changing the solid-to-porous ratio in the selected cases when comparing the stiffness of the implant-bone system. In the finite element models, the porous parts were modelled through the material properties, meaning that the computational study assessed the ratio without taking into account the reduced contact area caused by the presence of the pores. The difference in Young's modulus when changing the solid-to-porous ratio was negligible. Many computational studies revealed the great influence of the cage footprint, being a greater contact area advantageous to reduce subsidence. This consideration could lead to the development of a more advanced finite element model that assesses stiffness with the presence of pores at the contact surface.

### 8-3 Standalone cage and fixation systems

Due to the tilting of the device, the end of test was reached more quickly than it would have by simulating with a fixation system, or with the surrounding anatomical structure present *in vivo*. In the lumbar cages, the tilting in these tests occurred above the physiological load, for the high-density foam at  $970 \pm 68$  N, for the medium-density foam at  $770 \pm 74$  N, and for the low-density at  $480 \pm 68$  N. The standard deviation found was most likely an effect of the variability given by the random pore location within the foams. In fact, in the animations generated with the DIC system, the tilt would visibly initiate with the sinking of one of the two sides in the pores. Therefore, it depended on the specific pore configuration beneath the cage and on the cell pore size in which it would gradually sink.

The cervical cage was designed to include a fixation system, which was not tested for the current study since the purpose was to evaluate the effect of device porosity. In the case

of the lumbar cage, the design did not include the openings for the screws, therefore it was thought to be used as a standalone device. Although the subsidence test, as clearly mentioned in the standard, was not meant to simulate the *in-vivo* performance, the tilting behaviour could still be significant for considering reevaluation of the cage design. Of course, in reality this device should host bone graft in the central space and also around it, making it more stable, but based on the information about the way the sinking happened in reported cases in the literature, it could be hypothesized that the instability given by a narrow footprint could cause the tilting of cages, leading to subsidence.

#### **8-4 ASTM-F2267: considerations and recommendations**

The offset displacements indicated by the standard varied according to the type of implant and were reportedly 1 mm for the cervical implant and 2 mm for the lumbar implant. For this study, the offset displacement for the lumbar cages was set to 1.5 mm to allow comparisons between the curves with different substrate density. In fact, by using the 2 mm offset displacement, there was no intersection between the force-displacement curve and the plotted line for the case with the lower density foam. The standard was made for the employment of a grade 15 polyurethane foam, corresponding to the medium-density substrate of this work. Consequently, it could be expected that the offset displacement could not be suitable for all the grades tested. The offset displacement had to be settled to allow an appropriate and scientifically relevant comparison between grades.

Furthermore, the current standard could be questionable for the lack of the assessment of subsidence using dynamic compression tests. Two studies by Suh et al. [17] and Chong et al. [107] added to their static experiments some tests done using cyclic loading of the systems, using the same materials as the ones suggested for the static compression. Although this seemed to be a reasonable solution to retrieve data for the dynamic behaviour of subsidence, this method could be arguable for what is stated in point 5.2 of ASTM-F1839 for the specification of polyurethane foams. The foam is not intended to mimic the properties of human and animal bone, but solely to provide a consistent and uniform material close to the properties of cancellous bone. This means that the dynamic characterization and behaviour of the foam should be far from what is found in the biological materials, thus making the results of such experiments useless until proven biomechanically or better yet against *in-vivo* findings. Despite this, it could be useful if the dynamic tests could be standardized in order to have a measure of comparison among the implants, instead of collecting in the literature a range of different tests with variable conditions, from which results become difficult to compare. A very important feature missing from the standard is a layer that could simulate the properties of the endplate. In the real surgical case, the endplate is prepared through curettage, since it helps triggering the fusion. At the same time it should be preserved as well as possible because it was demonstrated that the failure load increases with the incremental removal of the endplate [36]. Of course, the standard states clearly that the tests are not representative of the real performance of the implants but the layer,

which has properties comparable to the cortical bone, has great impact and influence from a mechanical point of view. Therefore an amendment to include a layer respecting the intended surgical procedure with a much higher Young's modulus between the cage and the foam block should be considered. In this study, some considerations were made to implement such a layer, but finally in order to have validated references in the literature, it was decided to follow the standard.



---

## Chapter 9

---

# Conclusion

Porous interbody fusion cages are being increasingly developed and employed, although in the literature the information is still limited, while there is a complete lack of clinical studies. More research should be done to improve this device, which has become more popular due to the technological advancements, but also as a result of the increase of the aging population. Many design parameters, as well as the physiological ones, are still to be assessed.

In this study the design parameters assessed were the porosity of the implant and the thickness of the frame in solid titanium, when combined with three different polyurethane foam densities to mimic different bone conditions. The investigation aimed to find optimal solutions to reduce the risk of subsidence in relation to its most influencing factor, which is bone mineral density.

### 9-1 Biomechanical study

The metrics used for the biomechanical investigation were the stiffness values for implants, foam and the combination of the two. The focus was set particularly on the stiffness of the implant-foam system since subsidence was assessed as the crosshead displacement at physiological loading. The core of the blocks during the testings of the implant-bone systems did not undergo deformations within the limit of the physiological load. Furthermore, within the same loading limit, the force-displacement curves recorded for the systems remained in the linear region. Subsidence at physiological loading was measured as the crosshead displacement, since there were no strains recorded in the blocks. Therefore, the investigation focused on the combinations of implant porosities and foam densities that could achieve the least amount of crosshead displacement as an indicator of subsidence reduction. It was hypothesized that a greater porosity would decrease the stiffness of the system, as a consequence of stress reduction at the interface. This study did not reveal changes in the stiffness of the implant nor of the

implant-foam system when changing the porosity of the inner core of the implants, for the two tested porosity values. On the other hand, the results were aligned with the findings in the literature regarding the influence of bone mineral density on subsidence. It was possible to quantify the change of stiffness for the polyurethane foam which is commonly used for biomechanical tests, and leave a reference for its use in future studies.

## 9-2 Computational study

This thesis work started exploring, through a finite element model, the variation of another design parameter, which was the thickness of the solid frame, typically found in porous implants to withstand the physiological loads. The frame thickness was thought to carry the majority of the load, and the evaluation of a range of solid-to-porous ratios of the implants could help explaining if the lack of stiffness variation could be attributed to such behaviour. Three values for the solid-to-porous ratios were employed for the computational study, which did not reveal changes in the stiffness of the implant-foam system, as opposed to the changes observed when evaluating the stiffness of the cages alone. Although greater differences were observed throughout the latter simulations, the changes were still below the values of standard deviations reported for the performed mechanical tests. Of course, the results of the mechanical tests could not be considered significant for the simulation being that the model used was simplified, but the order of magnitude of the results was used to make these considerations.

## 9-3 Implications for the *in-vivo* performance of the implants

Although the variations in these design parameters were not found to improve mechanically the implant to avoid subsidence, the lack of changes in the mechanical performance indicates the possibility to focus studies on biological osseointegration by designing functionally graded lattices, for instance, without the risk of incurring in weaker cages that would not withstand the compressive forces in the spine.

---

## Chapter 10

---

# Recommendations

### 10-1 Assessment of the implant location

Further investigation should be carried out to make subsidence evaluation based on the different locations within the vertebral body. Oxland et al. [126] highlighted the differences in stiffness and strength magnitudes within the endplate. More specifically the posterior region was identified as stronger than the anterior one, while the overall peripheral region was stronger than the central area of the endplate. These findings are interesting to consider since they could help to exploit the bone regions accordingly and reduce the risk of subsidence. For instance, since partial endplate removal is necessary for fusion, it would be better to take parts from the centre instead of the strongest peripheral region.

### 10-2 Assessment of bone mineral density

A preliminary assessment of the bone density would be a great way to predict the risk of subsidence and to investigate possible solutions. An example is provided by Schreiber's work [125], in which correlations were obtained between Hounsfield units and BMD, enabling identification of patients with diminished bone density. Polyurethane foam was used to execute biomechanical experiments, revealing correlations between HU and compressive strength.

Many clinical studies are available in the literature reporting statistics about subsidence, but none of them collected data on the bone condition in patients. It would be useful to analyze the correlation between subsidence and bone mineral density in real cases and further advance in surgical solutions.

### **10-3 Cell proliferation and growth**

The next step for the research of porous spinal solutions should be the investigation of the osseointegration possibility of the implants used for this thesis. It could be interesting to make some biological evaluation with two lattices using the apparent densities of this work, both separately and in combination for a functionally graded lattice, as suggested by Van Bael et al [115]. Studies on osseointegration are generally conducted with scaffolds of simple geometry, but it would be interesting to evaluate cell proliferation and growth in the porous core of the implant.

More specifically, human femoral osteoblasts, human vertebral mesenchymal stem cells, and mouse preosteoblasts cultures could be considered on the titanium implants and compared in the proliferation and osteogenic differentiation of cells in the two porosity cases.

### **10-4 Biomechanical study**

The compression test used to evaluate cage subsidence is standardized in ASTM-F2267, which does not take into account the fatigue life of the implant. It would be interesting to further study the dynamic performance of the cage by developing a fatigue test protocol under physiological loading. Furthermore, the standard does not take into account the presence of the endplate at the interface with the implant, but uses the polyurethane foam which mimics the contact with trabecular bone. A future investigation could include a material that can model cancellous bone at the interface between implant and polyurethane foam. Before this step it would be necessary to investigate and validate which material could be suitable to model the endplate.

### **10-5 Computational study**

The finite element model built for the current study was simplified since it served as an exploratory model. It would be interesting to assess the influence of the teeth of the cage, that on the one hand could create great stress concentrations on the tips, but on the other hand could increase the contact area at the interface. More refined computational studies shall then include the implant teeth, together with plasticity in the material modelling, since indentation would be expected. Furthermore, the influence of tangential forces, as a consequence of the draft angle of the cage, shall be included to understand the role of friction between the surfaces.

---

# Bibliography

- [1] Spine Universe, “The structure of the segments of the spine.”
- [2] P. P. Raj, “Intervertebral Disc: Anatomy-Physiology-Pathophysiology-Treatment,” *Pain Practice*, vol. 8, pp. 18–44, 1 2008.
- [3] Mayo Clinic, “Herniated lumbar disc,” 2018.
- [4] Mayo Clinic, “Spinal stenosis,” 2018.
- [5] A. F. Gaillard, “Spondylolisthesis grading (illustration).”
- [6] American Academy of Orthopaedic Surgeons, “Interbody fusion.”
- [7] R. J. Mobbs, K. Phan, G. Malham, K. Seex, and P. J. Rao, “Lumbar interbody fusion: techniques, indications and comparison of interbody fusion options including PLIF, TLIF, MI-TLIF, OLIF/ATP, LLIF and ALIF.,” *Journal of spine surgery (Hong Kong)*, vol. 1, pp. 2–18, 12 2015.
- [8] Paradigm Spine, “Introducing a Non-Fusion Alternative for Lumbar Spinal Stenosis in the ASC,” 2018.
- [9] R. B. Cloward, “The treatment of ruptured lumbar intervertebral discs by vertebral body fusion,” *Journal of Neurosurgery: Spine*, 1952.
- [10] S. Kuslich, C. Ulstrom, S. Griffith, J. Ahern, and J. Dowdle, “The Bagby and Kuslich Method of Lumbar Interbody Fusion: History, Techniques, and 2-Year Follow-up Results of a United States Prospective, Multicenter Trial,” *Spine*, vol. 23(11), pp. 1267–1278, 1998.
- [11] Stryker, “Tempus,” 2018.
- [12] P. Barsa and P. Suchomel, “Factors affecting sagittal malalignment due to cage subsidence in standalone cage assisted anterior cervical fusion.,” *European spine*

- journal : official publication of the European Spine Society, the European Spinal Deformity Society, and the European Section of the Cervical Spine Research Society*, vol. 16, pp. 1395–400, 9 2007.
- [13] ASTM, “F-2267 Standard Test Method for Measuring Load Induced Subsidence of Intervertebral Body,” Tech. Rep. Reapproved, ASTM, 2004.
- [14] S. M. Ahmadi, G. Campoli, S. Amin Yavari, B. Sajadi, R. Wauthle, J. Schrooten, H. Weinans, and A. A. Zadpoor, “Mechanical behavior of regular open-cell porous biomaterials made of diamond lattice unit cells,” *Journal of the Mechanical Behavior of Biomedical Materials*, vol. 34, pp. 106–115, 2014.
- [15] Science for all Brainwaves, “Wettability.”
- [16] Pharmacy Haven, “Osteoporosis.”
- [17] P. B. Suh, C. Puttlitz, C. Lewis, B. S. Bal, and K. McGilvray, “The effect of cervical interbody cage morphology, material composition, and substrate density on cage subsidence,” *Journal of the American Academy of Orthopaedic Surgeons*, vol. 25, no. 2, pp. 160–168, 2017.
- [18] B. L. Riggs, K. P. Offord, L. J. Melton, H. W. Wahner, W. L. Dunn, and R. B. Mazess, “Differential changes in bone mineral density of the appendicular and axial skeleton with aging: relationship to spinal osteoporosis,” *J Clin Invest*, vol. 67, no. 2, p. 328, 1981.
- [19] P. D. D. H. K. B. P. E. J. J. E. J. O. K. Kelly A. Young, James A. Wise, *Anatomy & Physiology*. OpenStax College, 1 ed., 2013.
- [20] Sawbones, “Biomechanical test materials and composite bones for test and validation studies..”
- [21] I. C. Stein, K. D. Than, K. S. Chen, A. C. Wang, and P. Park, “Failure of a polyether-ether-ketone expandable interbody cage following transforaminal lumbar interbody fusion,” *European Spine Journal*, vol. 24, pp. 555–559, 5 2015.
- [22] P. D. Kim, E. M. Baron, and M. Levesque, “Extrusion of Expandable Stacked Interbody Device for Lumbar Fusion Case Report of a Complication,” *CASE REPORT SPINE*, vol. 37, no. 18, pp. 1155–1158, 2012.
- [23] FDA, “MAUDE - Manufacturer and User Facility Device Experience.”
- [24] “Amber Implants.”
- [25] Q. Zhang, Z. Yuan, M. Zhou, H. Liu, Y. Xu, and Y. Ren, “A comparison of posterior lumbar interbody fusion and transforaminal lumbar interbody fusion: a literature review and meta-analysis,” *BMC Musculoskeletal Disorders*, vol. 15, p. 367, 12 2014.

- 
- [26] C.-C. Hsu, "Shape optimization for the subsidence resistance of an interbody device using simulation-based genetic algorithms and experimental validation," *Journal of Orthopaedic Research*, vol. 31, pp. 1158–1163, 7 2013.
- [27] K. Siemionow, H. An, K. Masuda, G. Andersson, and G. Cs-Szabo, "The effects of age, sex, ethnicity, and spinal level on the rate of intervertebral disc degeneration: a review of 1712 intervertebral discs.," *Spine*, vol. 36, pp. 1333–9, 8 2011.
- [28] N. Boos, S. Weissbach, H. Rohrbach, C. Weiler, K. F. Spratt, and A. G. Nerlich, "Classification of age-related changes in lumbar intervertebral discs," *Spine*, vol. 27, no. 23, pp. 2631–2644, 2002.
- [29] N. G. Lasanianos, G. K. Triantafyllopoulos, and S. G. Pneumaticos, "Intervertebral Disc Herniation," in *Trauma and Orthopaedic Classifications: A Comprehensive Overview* (N. G. Lasanianos, N. K. Kanakaris, and P. V. Giannoudis, eds.), pp. 243–245, London: Springer London, 2015.
- [30] M. A. Adams and P. J. Roughley, "What is Intervertebral Disc Degeneration, and What Causes It?," *Spine*, vol. 31, pp. 2151–2161, 8 2006.
- [31] K. Luoma, H. Riihimaki, R. Luukkonen, R. Raininko, E. Viikari-Juntura, and A. Lamminen, "Low Back Pain in Relation to Lumbar Disc Degeneration," *Spine*, 2000.
- [32] J. M. Fritz, A. Delitto, W. C. Welch, and R. E. Erhard, "Lumbar spinal stenosis: A review of current concepts in evaluation, management, and outcome measurements," *Archives of Physical Medicine and Rehabilitation*, vol. 79, pp. 700–708, 6 1998.
- [33] P. H. Newman, "Spondylolisthesis, its cause and effect.," *Annals of the Royal College of Surgeons of England*, vol. 16, pp. 305–23, 5 1955.
- [34] R. Gunzburg and M. Szpalski, "The conservative surgical treatment of lumbar spinal stenosis in the elderly," *European Spine Journal*, vol. 12, pp. S176–S180, 10 2003.
- [35] A. Polikeit, S. J. Ferguson, L. P. Nolte, and T. E. Orr, "The importance of the endplate for interbody cages in the lumbar spine," *European Spine Journal*, vol. 12, no. 6, pp. 556–561, 2003.
- [36] L. Th, K. H, J. Ch, K. Jg, S. M, N. R, A. Hs, and A. Gb, "Effect of endplate conditions and bone mineral density on the compressive strength of the graft-endplate interface in anterior cervical spine fusion," *Spine*, vol. 26, no. 8, pp. 951–956, 2001.
- [37] R. D. Fraser, "Interbody, posterior, and combined lumbar fusions.," *Spine*, vol. 20, pp. 167S–177S, 12 1995.
- [38] L. Hackenberg, H. Halm, V. Bullmann, V. Vieth, M. Schneider, and U. Liljenqvist, "Transforaminal lumbar interbody fusion: a safe technique with satisfactory three to five year results," *European Spine Journal*, vol. 14, pp. 551–558, 8 2005.

- [39] L. Proietti, L. Scaramuzzo, G. R. Schiro', S. Sessa, and C. A. Logroscino, "Complications in lumbar spine surgery: A retrospective analysis.," *Indian journal of orthopaedics*, vol. 47, pp. 340–5, 7 2013.
- [40] K. Thomsen, "The Effect of Pedicle Screw Instrumentation on Functional Outcome and Fusion Rates in Posterolateral Lumbar Spinal Fusion: A Prospective Randomized Clinical Study.pdf," 1997.
- [41] F. Christensen Bjarke, E. Stender Hansen, M. Laursen, K. Thomsen, and C. Bunger, "Long-term functional outcome of pedicle screw instrumentation as a support for posterolateral spinal fusion: randomized clinical study with a 5-year follow-up," *Spine*, vol. 27(12), pp. 1269–1277, 2002.
- [42] D. Grob, A. Benini, A. Junge, and A. Mannion, "Clinical experience with the Dynesys semirigid fixation system for the lumbar spine: surgical and patient-oriented outcome in 50 cases after an average of 2 years," *Spine*, vol. 30(3), pp. 324–331, 2005.
- [43] I. Teng, J. Han, K. Phan, and R. Mobbs, "A meta-analysis comparing ALIF, PLIF, TLIF and LLIF," *Journal of Clinical Neuroscience*, vol. 44, pp. 11–17, 10 2017.
- [44] E. Truumees, K. Majid, and M. Brkaric, "Anterior Lumbar Interbody Fusion in the Treatment of Mechanical Low Back Pain," *Seminars in Spine Surgery*, vol. 20, no. 2, pp. 113–125, 2008.
- [45] G. Giang, R. Mobbs, S. Phan, T. M. Tran, and K. Phan, "Evaluating Outcomes of Stand-Alone Anterior Lumbar Interbody Fusion: A Systematic Review," *World Neurosurgery*, vol. 104, pp. 259–271, 8 2017.
- [46] B. M. Ozgur, H. E. Aryan, L. Pimenta, and W. R. Taylor, "Extreme Lateral Interbody Fusion (XLIF): a novel surgical technique for anterior lumbar interbody fusion," *The Spine Journal*, vol. 6, pp. 435–443, 7 2006.
- [47] S.-w. Fan, Z.-j. Hu, X.-q. Fang, F.-d. Zhao, Y. Huang, and H.-j. Yu, "Comparison of paraspinal muscle injury in one-level lumbar posterior inter-body fusion: modified minimally invasive and traditional open approaches," *Orthopaedic Surgery*, vol. 2, pp. 194–200, 7 2010.
- [48] S. Craig Humphreys, S. D. Hodges, A. G. Patwardhan, J. C. Eck, R. Bryan Murphy, and L. A. Covington, "Comparison of posterior and transforaminal approaches to lumbar interbody fusion," *Spine*, vol. 26(5), pp. 567–571, 2001.
- [49] N. Sakeb and K. Ahsan, "Comparison of the early results of transforaminal lumbar interbody fusion and posterior lumbar interbody fusion in symptomatic lumbar instability.," *Indian journal of orthopaedics*, vol. 47, pp. 255–63, 5 2013.
- [50] J. S. Park, Y. B. Kim, H. J. Hong, and S. N. Hwang, "Comparison between Posterior and Transforaminal Approaches for Lumbar Interbody Fusion.," *Journal of Korean Neurosurgical Society*, vol. 37, no. 5, pp. 340–344, 2005.

- 
- [51] A. S. Hilibrand and M. Robbins, "Adjacent segment degeneration and adjacent segment disease: the consequences of spinal fusion?," *The Spine Journal*, vol. 4, pp. S190–S194, 11 2004.
- [52] J. Y. Yang, J.-K. Lee, and H.-S. Song, "The Impact of Adjacent Segment Degeneration on the Clinical Outcome After Lumbar Spinal Fusion," *Spine*, vol. 33, pp. 503–507, 3 2008.
- [53] T. Miwa, H. Sakaura, T. Yamashita, S. Suzuki, and T. Ohwada, "Surgical outcomes of additional posterior lumbar interbody fusion for adjacent segment disease after single-level posterior lumbar interbody fusion," *European Spine Journal*, vol. 22, pp. 2864–2868, 12 2013.
- [54] M. Kumar, A. Baklanov, and D. Chopin, "Correlation between sagittal plane changes and adjacent segment degeneration following lumbar spine fusion," *European Spine Journal*, vol. 10, pp. 314–319, 8 2001.
- [55] J. M., L. C., and B. R., "Outcomes of allogenic cages in anterior and posterior lumbar interbody fusion," *European Spine Journal*, vol. 10, pp. S158–S168, 10 2001.
- [56] R. Rothman, "Failures of spinal fusion," *Spine*, vol. 6, pp. 299–304, 1975.
- [57] C. Lee, J. Dorcil, and T. E. Radomisli, "Nonunion of the Spine," *Clinical Orthopaedics and Related Research*, vol. 419, no. 419, pp. 71–75, 2004.
- [58] C. Xu, W.-F. Ni, N.-F. Tian, X.-Q. Hu, F. Li, and H.-Z. Xu, "Complications in degenerative lumbar disease treated with a dynamic interspinous spacer (Coflex)," *International Orthopaedics*, vol. 37, pp. 2199–2204, 11 2013.
- [59] S. Christie, J. Song, and R. G. Fessler, "Dynamic interspinous process technology," *Spine*, vol. 30, no. 16 SUPPL., pp. S73–S78, 2005.
- [60] A. Nachanakian, A. El Helou, and M. Alaywan, "The interspinous spacer: a new posterior dynamic stabilization concept for prevention of adjacent segment disease.," *Advances in orthopedics*, vol. 2013, p. 637362, 4 2013.
- [61] A. Landi, "Interspinous posterior devices: What is the real surgical indication?," *World journal of clinical cases*, vol. 2, pp. 402–8, 9 2014.
- [62] K. Phan, P. J. Rao, J. R. Ball, and R. J. Mobbs, "Interspinous process spacers versus traditional decompression for lumbar spinal stenosis: systematic review and meta-analysis.," *Journal of spine surgery (Hong Kong)*, vol. 2, pp. 31–40, 3 2016.
- [63] G. W. Bagby, "Arthrodesis by the distraction-compression method using a stainless steel implant," *Orthopedics*, vol. 6, pp. 931–934, 1988.
- [64] R. J. Mobbs, A. Loganathan, V. Yeung, and P. J. Rao, "Indications for Anterior Lumbar Interbody Fusion," *Orthopaedic Surgery*, vol. 5, pp. 153–163, 8 2013.

- [65] J. D. Coe, J. F. Zucherman, D. W. Kucharzyk, K. A. Poelstra, L. E. Miller, and S. Kunwar, "Multiexpandable cage for minimally invasive posterior lumbar interbody fusion.," *Medical devices (Auckland, N.Z.)*, vol. 9, pp. 341–347, 2016.
- [66] G. N. Rymarczuk, J. S. Harrop, A. Hilis, and R. Härtl, "Should expandable TLIF cages be used routinely to increase lordosis?," *Clinical Spine Surgery*, vol. 30, no. 2, pp. 47–49, 2017.
- [67] M. Alimi, B. Shin, M. Macielak, C. P. Hofstetter, I. Njoku, A. J. Tsiouris, E. Elowitz, R. Härtl, and R. Härtl, "Expandable Polyaryl-Ether-Ether-Ketone Spacers for Interbody Distraction in the Lumbar Spine.," *Global spine journal*, vol. 5, pp. 169–78, 6 2015.
- [68] G. Gu, H. Zhang, G. Fan, S. He, X. Cai, X. Shen, X. Guan, and X. Zhou, "Comparison of minimally invasive versus open transforaminal lumbar interbody fusion in two-level degenerative lumbar disease," *International Orthopaedics*, vol. 38, pp. 817–824, 4 2014.
- [69] Y. M. Gussous, N. Jain, and S. N. Khan, "Posterior based lumbar interbody fusion devices: Static and expandable technology," *Seminars in Spine Surgery*, 2018.
- [70] P. J. Rao, M. H. Pelletier, W. R. Walsh, and R. J. Mobbs, "Spine Interbody Implants: Material Selection and Modification, Functionalization and Bioactivation of Surfaces to Improve Osseointegration," *Orthopaedic Surgery*, vol. 6, pp. 81–89, 5 2014.
- [71] R. Thull, "Surface treatment," *Metals for Biomedical Devices*, pp. 251–259, 1 2010.
- [72] J. D. Bobyn, E. S. Mortimer, A. H. Glassman, C. A. Engh, J. E. Miller, and C. E. Brooks, "Producing and avoiding stress shielding. Laboratory and clinical observations of noncemented total hip arthroplasty.," *Clinical orthopaedics and related research*, pp. 79–96, 1 1992.
- [73] S. Seaman, P. Kerezoudis, M. Bydon, J. C. Torner, and P. W. Hitchon, "Titanium vs. polyetheretherketone (PEEK) interbody fusion: Meta-analysis and review of the literature," *Journal of Clinical Neuroscience*, vol. 44, pp. 23–29, 2017.
- [74] S. M. Kurtz and J. N. Devine, "PEEK biomaterials in trauma, orthopedic, and spinal implants," *Biomaterials*, vol. 28, pp. 4845–4869, 11 2007.
- [75] R. F. M. R. Kersten, S. M. Van Gaalen, A. De Gast, and F. C. Öner, "Polyetheretherketone (PEEK) cages in cervical applications: A systematic review," *Spine Journal*, vol. 15, no. 6, pp. 1446–1460, 2015.
- [76] T. Hashimoto, K. Shigenobu, M. Kanayama, M. Harada, F. Oha, Y. Ohkoshi, H. Tada, K. Yamamoto, and S. Yamane, "Clinical results of single-level posterior lumbar interbody fusion using the Brantigan I/F carbon cage filled with a mixture

- of local morselized bone and bioactive ceramic granules,” *Spine*, vol. 27, no. 3, pp. 258–262, 2002.
- [77] B. Jost, P. A. Cripton, T. Lund, T. R. Oxland, K. Lippuner, P. Jaeger, and L.-P. Nolte, “Compressive strength of interbody cages in the lumbar spine: the effect of cage shape, posterior instrumentation and bone density,” *European Spine Journal*, vol. 7, pp. 132–141, 5 1998.
- [78] D. Mahmoud, M. Elbestawi, D. Mahmoud, and M. A. Elbestawi, “Lattice Structures and Functionally Graded Materials Applications in Additive Manufacturing of Orthopedic Implants: A Review,” *Journal of Manufacturing and Materials Processing*, vol. 1, p. 13, 10 2017.
- [79] L. S. Chatham, V. V. Patel, C. M. Yakacki, and R. Dana Carpenter, “Interbody Spacer Material Properties and Design Conformity for Reducing Subsidence During Lumbar Interbody Fusion,” *Journal of biomechanical engineering*, vol. 139, p. 0510051, 5 2017.
- [80] W. Pompe, H. Worch, M. Epple, W. Friess, M. Gelinsky, P. Greil, U. Hempel, D. Scharnweber, and K. Schulte, “Functionally graded materials for biomedical applications,” *Materials Science and Engineering: A*, vol. 362, pp. 40–60, 12 2003.
- [81] R. A. Gittens, R. Olivares-Navarrete, Z. Schwartz, and B. D. Boyan, “Implant osseointegration and the role of microroughness and nanostructures: Lessons for spine implants,” *Acta Biomaterialia*, vol. 10, pp. 3363–3371, 8 2014.
- [82] A. Wennerberg and T. Albrektsson, “Effects of titanium surface topography on bone integration: a systematic review,” *Clinical Oral Implants Research*, vol. 20, pp. 172–184, 9 2009.
- [83] E. Garner, H. M. Kolken, C. C. Wang, A. A. Zadpoor, and J. Wu, “Compatibility in microstructural optimization for additive manufacturing,” *Additive Manufacturing*, vol. 26, pp. 65–75, 3 2019.
- [84] J. Havlikova, J. Strasky, M. Vandrovцова, P. Harcuba, M. Mhaede, M. Janecek, and L. Bacakova, “Innovative surface modification of Ti-6Al-4V alloy with a positive effect on osteoblast proliferation and fatigue performance,” *Materials Science and Engineering: C*, vol. 39, pp. 371–379, 6 2014.
- [85] P. R. Klokkevold, R. D. Nishimura, M. Adachi, and A. Caputo, “Osseointegration enhanced by chemical etching of the titanium surface. A torque removal study in the rabbit,” *Clinical Oral Implants Research*, vol. 8, pp. 442–447, 12 1997.
- [86] B. P. Dahl Gehrchen P Blyme T Ki, e. E. Tondevold, B. N. Dahl, and M. T. Gehrchen P Blyme Kia, “Clinical outcome after spinal fusion with a rigid versus a semi-rigid pedicle screw system,” *Eur Spine J*, vol. 6, pp. 412–416, 1997.
- [87] D. S. Shin, K. Lee, and D. Kim, “Biomechanical study of lumbar spine with dynamic stabilization device using finite element method,” *Computer-Aided Design*, vol. 39, pp. 559–567, 7 2007.

- [88] S. Y. Han, H. W. Kim, C. Y. Lee, H. R. Kim, and D. H. Park, "Stand-Alone Cages for Anterior Cervical Fusion: Are There No Problems?," *Korean Journal of Spine*, vol. 13, pp. 13–9, 3 2016.
- [89] E. Gercek, V. Arlet, J. Delisle, and D. Marchesi, "Subsidence of stand-alone cervical cages in anterior interbody fusion: warning," *European Spine Journal*, vol. 12, pp. 513–516, 10 2003.
- [90] E. Emstad, D. C. del Monaco, L. C. Fielding, and J. E. Block, "The VariLift® Interbody Fusion System: Expandable, standalone interbody fusion," *Medical Devices: Evidence and Research*, vol. 8, pp. 219–230, 2015.
- [91] W. F. Neely, F. Fichtel, D. C. del Monaco, and J. E. Block, "Treatment of Symptomatic Lumbar Disc Degeneration with the VariLift-L Interbody Fusion System: Retrospective Review of 470 Cases," *International Journal of Spine Surgery*, vol. 10, p. 15, 1 2016.
- [92] P. C. McAfee, B. W. Cunningham, G. A. Lee, C. M. Orbegoso, C. J. Haggerty, I. L. Fedder, and S. L. Griffith, "Revision Strategies for Salvaging or Improving Failed Cylindrical Cages," *Spine*, vol. 24, pp. 2147–2153, 1999.
- [93] L. Chen, H. Yang, and T. Tang, "Cage migration in spondylolisthesis treated with posterior lumbar interbody fusion using BAK cages," *Spine*, vol. 30(19), pp. 2171–2175, 2005.
- [94] J. Y. Choi and K. H. Sung, "Subsidence after anterior lumbar interbody fusion using paired stand-alone rectangular cages," *European Spine Journal*, vol. 15, pp. 16–22, 2 2006.
- [95] B. Godlewski, M. K. Stachura, R. A. Czepko, M. Banach, and R. Czepko, "Analysis of changes in cervical spinal curvature and intervertebral disk space height following ACDF surgery in a group of 100 patients followed up for 12 months," *Journal of Clinical Neuroscience*, vol. 52, pp. 92–99, 6 2018.
- [96] C. W. Kim, T. M. Doerr, I. Y. Luna, G. Joshua, S. R. Shen, X. Fu, and A.-M. Wu, "Minimally Invasive Transforaminal Lumbar Interbody Fusion Using Expandable Technology: A Clinical and Radiographic Analysis of 50 Patients," *World Neurosurgery*, vol. 90, pp. 228–235, 6 2016.
- [97] E. Truumees, C. K. Demetropoulos, K. H. Yang, and H. N. Herkowitz, "Effects of disc height and distractive forces on graft compression in an anterior cervical corpectomy model," *Spine*, vol. 33, no. 13, pp. 1438–1441, 2008.
- [98] Z. Zhang, H. Li, G. R. Fogel, Z. Liao, Y. Li, and W. Liu, "Biomechanical Analysis of Porous Additive Manufactured Cages for Lateral Lumbar Interbody Fusion: A Finite Element Analysis," *World Neurosurgery*, vol. 111, pp. e581–e591, 3 2018.
- [99] M. Attaran, "The rise of 3-D printing: The advantages of additive manufacturing over traditional manufacturing," *Business Horizons*, vol. 60, pp. 677–688, 9 2017.

- 
- [100] P. S. D'Urso, O. D. Williamson, and R. G. Thompson, "Biomodeling as an aid to spinal instrumentation," *Spine*, vol. 30, no. 24, pp. 2841–2845, 2005.
- [101] M. T. Izatt, P. L. P. J. Thorpe, R. G. Thompson, P. S. D'Urso, C. J. Adam, J. W. S. Earwaker, R. D. Labrom, and G. N. Askin, "The use of physical biomodelling in complex spinal surgery," *European Spine Journal*, vol. 16, pp. 1507–1518, 9 2007.
- [102] W. J. Choy, W. C. H. Parr, K. Phan, W. R. Walsh, and R. J. Mobbs, "3-dimensional printing for anterior cervical surgery: a review.," *Journal of spine surgery (Hong Kong)*, vol. 4, pp. 757–769, 12 2018.
- [103] ASTM, "F-2077 Test Methods For Intervertebral Body Fusion Devices," tech. rep., ASTM, 2015.
- [104] J. Graham and B. T. Estes, "What standards can (and can't) tell us about a spinal device," *ESAS*, vol. 3, pp. 178–183, 2009.
- [105] W. Schmoelz and A. Kienle, "Mechanical and Biomechanical Testing of Spinal Implants," in *Manual of Spine Surgery*, pp. 23–26, Berlin, Heidelberg: Springer Berlin Heidelberg, 2012.
- [106] ASTM International, "F1839-08: Standard Specification for Rigid Polyurethane Foam for use as a Standard Material for Testing Orthopaedic Devices and Instruments," *Annual Book of ASTM Standards*, vol. 08, no. Reapproved 2012, pp. 6–11, 2014.
- [107] A. C. M. Chong, S. W. Harrer, M. H. Heggeness, and P. H. Wooley, "Biomechanical evaluation of CIBOR spine interbody fusion device," *J Biomed Mater Res Part B: Appl Biomater*, vol. 105, pp. 1157–1168, 2016.
- [108] G. Sung, H. Choe, Y. Choi, and J. H. Kim, "Morphological, acoustical, and physical properties of free-rising polyurethane foams depending on the flow directions," *Korean Journal of Chemical Engineering*, vol. 35, pp. 1045–1052, 4 2018.
- [109] K. L. Calvert, K. P. Trumble, T. J. Webster, and L. A. Kirkpatrick, "Characterization of commercial rigid polyurethane foams used as bone analogs for implant testing," *Journal of Materials Science: Materials in Medicine*, vol. 21, pp. 1453–1461, 5 2010.
- [110] N. R. Ordway, B. C. Rim, R. Tan, R. Hickman, and A. H. Fayyazi, "Anterior cervical interbody constructs: effect of a repetitive compressive force on the endplate," *Journal of Orthopaedic Research*, vol. 30, pp. 587–592, 4 2012.
- [111] J. Choi, D.-A. Shin, and S. Kim, "Biomechanical Effects of the Geometry of Ball-and-Socket Artificial Disc on Lumbar Spine: A Finite Element Study.," *Spine*, vol. 42, pp. E332–E339, 3 2017.
- [112] M. Niinomi, "Mechanical properties of biomedical titanium alloys," *Materials Science and Engineering: A*, vol. 243, pp. 231–236, 3 1998.

- [113] S. Amin Yavari, S. M. Ahmadi, R. Wauthle, B. Pouran, J. Schrooten, H. Weinans, and A. A. Zadpoor, "Relationship between unit cell type and porosity and the fatigue behavior of selective laser melted meta-biomaterials," *Journal of the Mechanical Behavior of Biomedical Materials*, vol. 43, pp. 91–100, 2015.
- [114] P.-I. Tsai, C.-C. Hsu, S.-Y. Chen, T.-H. Wu, and C.-C. Huang, "Biomechanical investigation into the structural design of porous additive manufactured cages using numerical and experimental approaches," *Computers in Biology and Medicine*, vol. 76, pp. 14–23, 9 2016.
- [115] S. Van Bael, Y. Chai, S. Truscello, M. Moesen, G. Kerckhofs, H. Van Oosterwyck, J.-P. Kruth, and J. Schrooten, "The effect of pore geometry on the in vitro biological behavior of human periosteum-derived cells seeded on selective laser-melted Ti6Al4V bone scaffolds," *Acta Biomaterialia*, vol. 8, pp. 2824–2834, 7 2012.
- [116] A. C. Jones, C. H. Arns, A. P. Sheppard, D. W. Huttmacher, B. K. Milthorpe, and M. A. Knackstedt, "Assessment of bone ingrowth into porous biomaterials using MICRO-CT," *Biomaterials*, vol. 28, pp. 2491–2504, 5 2007.
- [117] M. Rumpler, A. Woesz, J. W. Dunlop, J. T. van Dongen, and P. Fratzl, "The effect of geometry on three-dimensional tissue growth," *Journal of The Royal Society Interface*, vol. 5, pp. 1173–1180, 10 2008.
- [118] C. Sittig, M. Textor, N. Spencer, M. Wieland, and P.-H. Vallotton, "Surface characterization of implant materials c.p. Ti, Ti-6Al-7Nb and Ti-6Al-4V with different pretreatments," *Journal of Materials Science: Materials in Medicine*, vol. 10, no. 1, pp. 35–46, 1999.
- [119] L. Le Guéhennec, A. Soueidan, P. Layrolle, and Y. Amouriq, "Surface treatments of titanium dental implants for rapid osseointegration," *Dental Materials*, vol. 23, no. 7, pp. 844–854, 2007.
- [120] C. Massaro, P. Rotolo, F. De Riccardis, E. Milella, A. Napoli, M. Wieland, M. Textor, N. Spencer, and D. Brunette, "Comparative investigation of the surface properties of commercial titanium dental implants. Part I: Chemical composition," *Journal of Materials Science: Materials in Medicine*, vol. 13, no. 6, pp. 535–548, 2002.
- [121] R. A. Gittens, R. Olivares-Navarrete, A. Cheng, D. M. Anderson, T. McLachlan, I. Stephan, J. Geis-Gerstorfer, K. H. Sandhage, A. G. Fedorov, F. Rupp, B. D. Boyan, R. Tannenbaum, and Z. Schwartz, "The roles of titanium surface micro/nanotopography and wettability on the differential response of human osteoblast lineage cells," *Acta Biomaterialia*, vol. 9, pp. 6268–6277, 4 2013.
- [122] A. Calvo-Echenique, J. Cegoñino, R. Chueca, and A. Pérez-del Palomar, "Stand-alone lumbar cage subsidence: A biomechanical sensitivity study of cage design and placement.," *Computer Methods and Programs in Biomedicine*, vol. 162, pp. 211–219, 8 2018.

- [123] Z.-C. Zhong, S.-H. Wei, J.-P. Wang, C.-K. Feng, C.-S. Chen, and C.-h. Yu, "Finite element analysis of the lumbar spine with a new cage using a topology optimization method," *Medical Engineering & Physics*, vol. 28, pp. 90–98, 1 2006.
- [124] S. S. Rajaei, H. W. Bae, L. E. A. Kanim, and R. B. Delamarter, "Spinal fusion in the United States: Analysis of trends from 1998 to 2008," *Spine*, vol. 37, no. 1, pp. 67–76, 2012.
- [125] J. J. Schreiber, P. A. Anderson, H. G. Rosas, A. L. Buchholz, and A. G. Au, "Hounsfield Units for Assessing Bone Mineral Density and Strength: A Tool for Osteoporosis Management," *The Journal of Bone and Joint Surgery-American Volume*, vol. 93, pp. 1057–1063, 6 2011.
- [126] T. R. Oxland, J. P. Grant, M. F. Dvorak, and C. G. Fisher, "Effects of Endplate Removal on the Structural Properties of the Lower Lumbar Vertebral Bodies," *Spine*, vol. 28, pp. 771–777, 4 2003.



---

# Glossary

## List of Acronyms

<b>AF</b>	annulus fibrosus
<b>ALIF</b>	anterior lumbar interbody fusion
<b>ASD</b>	Adjacent segment degeneration
<b>ASTM</b>	American Society for Testing and Material
<b>BMD</b>	bone mineral density
<b>CE</b>	chemical etching
<b>CFRP</b>	carbon fiber reinforced polymers
<b>DIC</b>	digital image correlation
<b>FDA</b>	Food and Drug Administration
<b>FSU</b>	functional spinal unit
<b>HU</b>	Hounsfield unit
<b>IVD</b>	intervertebral disc
<b>LBP</b>	low back pain
<b>LLIF</b>	lateral lumbar interbody fusion
<b>NP</b>	nucleus pulposus
<b>PLIF</b>	posterior lumbar interbody fusion
<b>ROM</b>	range of motion
<b>TLIF</b>	transforaminal lumbar interbody fusion

